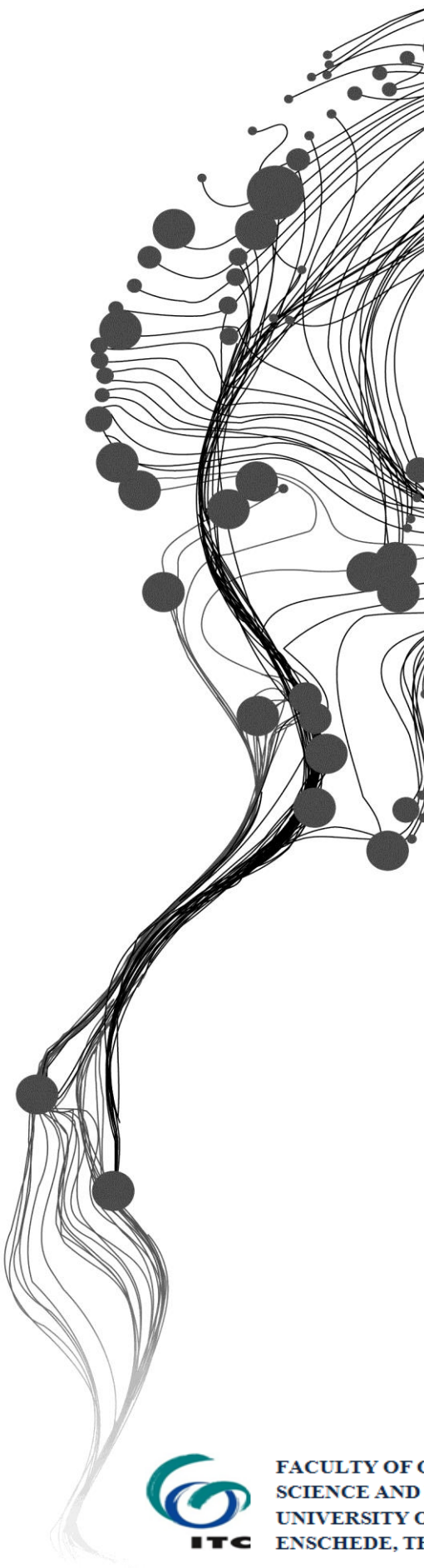


Hybrid Polarimetric Decomposition for Aboveground Biomass Estimation using Semi- empirical Modelling

KILEDAR SINGH TOMAR
March, 2015

ITC SUPERVISOR
Dr. Valentyn Tolpekin

IIRS SUPERVISOR
Mr. Shashi Kumar



Hybrid Polarimetric Decomposition for Aboveground Biomass Estimation using Semi- empirical Modelling

Kiledar Singh Tomar

Enschede, the Netherlands [March, 2015]

Thesis submitted to the Faculty of Geo-information Science and Earth Observation of the University of Twente in partial fulfilment of the requirements for the degree of Master of Science in Geo-information Science and Earth Observation.
Specialization: Geoinformatics.

THESIS ASSESSMENT BOARD:

Chairperson : Prof. Dr. Ir. M. G. Vosselman
ITC Professor : Prof. Dr. Ir. A. Stein
External Examiner : Mr. Sanjay (DEAL, Dehradun)
ITC Supervisor : Dr. Valentyn Tolpekin
IIRS Supervisor : Mr. Shashi Kumar

OBSERVERS:

ITC Observer : Dr. Nicholas Hamm
IIRS Observer : Dr. S. K. Srivastav



**FACULTY OF GEO-INFORMATION
SCIENCE AND EARTH OBSERVATION,
UNIVERSITY OF TWENTE,
ENSCHDEDE, THE NETHERLANDS**



INDIAN INSTITUTE OF REMOTE SENSING
Indian Space Research Organisation
Department of Space, Government of India

DISCLAIMER

This document describes work undertaken as part of a programme of study at the Faculty of Geo-information Science and Earth Observation (ITC), University of Twente, The Netherlands. All views and opinions expressed therein remain the sole responsibility of the author, and do not necessarily represent those of the institute.

Dedicated to my loving father...

Shri Mahendra Pratap Singh Tomar

ABSTRACT

Forest covers two-third of land cover and are considered most diversified form of ecosystem. Forests helps in preserving global carbon balance by acting as either carbon sink or source. The imbalance in carbon leads to climate change which is an exigent issue. Scrutinising the forest biomass is imperative in assessing the variation in climate because of the imbalance in carbon cycle. To quantify rapid change in forest biomass remote sensing techniques plays a crucial role. Previous research evaluated the potential of fully polarimetric data to monitor forest biomass. This work deals with the forest biomass estimation using FRS-1 mode of RISAT-1 and its comparison with the RADARSAT-2 fully polarimetric data and field measured biomass. The study was conducted in Sal dominating Barkot Forest. The research work intends to derive parameters from m-chi, m-alpha, m-delta and Yamaguchi decomposition techniques. The semi-empirical model is Extended Water Cloud Model (EWCM) is used to derive biomass with the parameters obtained from the decomposition techniques. The in-situ measurements were performed to estimate field biomass. In this context a comparative analysis was done between modelled biomass and field biomass. The R^2 values for modelled biomass against field biomass with m-delta, m-alpha, m-delta and Yamaguchi decomposition came out to be 0.3977, 0.4677, 0.5127 and 0.4625 respectively. The accuracy assessment was done using Root Mean Square Error (RMSE) which was found to be 64.422 ($t\ ha^{-1}$), 45.995 ($t\ ha^{-1}$), 63.156 ($t\ ha^{-1}$) and 73.124 ($t\ ha^{-1}$) corresponding to m-delta, m-alpha, m-delta and Yamaguchi decomposition techniques respectively. Significant correlation was found between the field biomass and the modelled biomass utilising m-chi decomposition. In addition, it was concluded that AGB estimation using Hybrid PolSAR data was viable than the AGB estimation using fully polarimetric data.

Keywords: Hybrid PolSAR, Fully PolSAR, Aboveground Biomass, Extended Water Cloud Model

ACKNOWLEDGEMENTS

This thesis arose as part of M.Sc. project work carried out in IIRS, India and ITC, Netherlands. This thesis would not have materialized without the guidance and support of many people who deserve a special mention.

I am especially thankful to my IIRS supervisor, Mr. Shashi Kumar, for his patient guidance without which this work would be impossible. The long hours of fruitful discussions has made me a better researcher and human being.

Special thanks to my ITC supervisor Dr. V. A. Tolpekin, for his unlimited support during my stay in ITC, Netherlands and his useful inputs during my thesis and proposal work. His constant feedback for my proposal helped me decide a true course for my thesis.

I would like to thank Dr. S.K. Srivastav for taking out time from his busy schedule and enquiring and providing useful and deep insight for the project work.

I would like to thank Mr. P.L.N. Raju for supporting me during the project work.

I am grateful to Dr. Y.V.N. Krishnamurthy, former Director IIRS for allowing me to be the part of the Masters program.

I would like to thank my seniors Mr. Deepak Chaudhary, Mr. Hemanth Konga, Mr. Abhishek Sobhana, Mr. Shashi Gaurav, Mr. Kanishk Chaturvedi, Mr. Ishaan Kochhar, Mr. Unmesh Khati, Mr. Raj Bhagat, Mr. Guru Pradhan, Mr. Arvind Hari, Mr. Ponraj Armugam, Mr. Hemant Bist and Mr. Rohit Kumar for helping in understanding tough concept and providing moral support during my tough days.

I would like to thank my M.Tech. Batch mates Sanjay, Pratiman, Richa, Surya, Harjeet, Ram, Raja, Rohit, Vikrant, Abhishek Das, Panini, Kavisha, Vineet, Joyson and Aniket.

I am grateful to my PG Diploma friends Minakshi, Sanjeev, Saifu, Boka, Chauksi, Sambhu Sir, Juna Di and Amit Sir.

I thank my M.Sc. friends Akshara, Saikia, Bhopali, Vanya and Pranay for their continuous support during ITC and IIRS stay.

I would also like to thank my Engineering Collage friends Bhoop Singh Tomar, Ashu Yadav, Sandeep Singh, Harsh, Dhakad, Manish, Miniraj, Gajendra, Akash Gupta, Gaurav Goyal, Santosh Verma and Bipin Verma for their helps and encouragement.

I would also like to thank my roommate Neeraj Agrawal (Bunny) and friend Shishant Gupta for his continuous support from the last eight years and to be with me.

I owe my heartfelt thanks to my parents, and my grandparents for their support and affection. They have been my greatest source of inspiration and support.

TABLE OF CONTENTS

1.	INTRODUCTION.....	1
1.1.	RADAR REMOTE SENSING	2
1.2.	PROBLEM STATEMENT AND MOTIVATION	5
1.3.	RESEARCH IDENTIFICATION	6
1.3.1.	Main Objective.....	6
1.3.2.	Sub-Objectives	6
1.4.	RESEARCH QUESTIONS	6
1.5.	INNOVATION AIMED AT.....	7
1.6.	STRUCTURE OF THE THESIS.....	7
2.	LITERATURE REVIEW.....	8
2.1.	SAMPLING PLAN FOR AGB ESTIMATION.....	8
2.2.	ROLE OF REMOTE SENSING FOR THE ESTIMATION OF AGB.....	9
2.2.1.	AGB Estimation using Active Remote Sensing.....	9
2.2.1.1.	AGB Estimation through Lidar.....	9
2.2.1.2.	AGB Estimation through SAR.....	10
2.3.	USE OF SAR POLARIMETRY IN AGB ESTIMATION	11
2.4.	HYBRID POLARIMETRY	13
2.5.	POLARIMETRIC DECOMPOSITION FOR THE ESTIMATION OF AGB.....	13
2.6.	MODEL BASED MEASUREMENT TO ESTIMATE THE AGB.....	14
3.	STUDY AREA.....	16
3.1.	INTRODUCTION	16
3.2.	BLOCK WISE DIVISION OF BARKOT FOREST	16
3.3.	STATEMENT OF SIGNIFICANCE	18
3.4.	CLIMATE.....	18
3.5.	SOIL.....	18
3.6.	FLORA.....	19
3.7.	FAUNA	19
4.	MATERIALS AND METHODS	20
4.1.	MATERIALS.....	20
4.1.1.	Satellite Data.....	20
4.1.2.	Field Data	20
4.1.3.	Calculations of field estimated AGB	21
4.1.3.1.	Basal Area	22

4.1.3.2.	Stem Volume.....	22
4.1.3.3.	Aboveground Biomass (AGB) estimation	22
4.2.	METHODOLOGY	23
4.3.	STOKES PARAMETERS	24
4.3.1.	Stokes Child Parameters.....	25
4.3.2.	Hybrid PolSAR Decomposition Modelling.....	26
4.3.2.1.	m-delta ($m-\delta$) decomposition.....	26
4.3.2.2.	m-chi ($m-\chi$) Decomposition	27
4.3.2.3.	m-alpha ($m-\alpha$) Decomposition.....	28
4.3.3.	Fully PolSAR Data Processing.....	28
4.3.3.1.	Generation of Scattering Matrix	29
4.3.3.2.	Decomposition of Scattering Matrix.....	29
4.3.3.3.	Decomposition Modelling.....	30
4.3.4.	Modelling Approach for AGB estimation.....	32
4.3.4.1.	Water Cloud Model (WCM).....	33
4.3.4.2.	Extended Water Cloud Model (EWCM).....	34
5.	RESULTS.....	38
5.1.	HYBRID POLARIMETRIC DECOMPOSITION COMPONENTS AND RESULTS.....	38
5.1.1.	m-delta ($m-\delta$) decomposition	38
5.1.2.	m-chi ($m-\chi$) decomposition.....	40
5.1.3.	m-alpha ($m-\alpha$) decomposition	41
5.2.	FULLY POLARIMETRIC DECOMPOSITION COMPONENTS AND RESULTS.....	43
5.3.	COMPARISONS OF DECOMPOSITION COMPONENTS.....	45
5.3.1.	Volume Scattering:	45
5.3.2.	Double Bounce Scattering:.....	45
5.3.3.	Surface Scattering:	46
5.4.	RELATIONSHIP BETWEEN VOLUME SCATTERING AND FIELD BIOMASS.....	47
5.5.	RELATIONSHIP BETWEEN TOTAL FOREST BACKSCATTER AND MEASURED BIOMASS	48
5.6.	PARAMETER ESTIMATION OF EWCM AND RESULTS	49
5.6.1.	Retrieval of β	49
5.6.2.	Retrieval of AGB using EWCM.....	50
5.7.	PERFORMANCE ANALYSIS.....	52
6.	DISCUSSION.....	54
7.	CONCLUSION AND RECOMMENDATIONS	57
7.1.	CONCLUSION	57

7.2. ANSWERS TO RESEARCH QUESTIONS	58
7.3. RECOMMENDATIONS	59
REFERENCES.....	60
APPENDIX A	65

LIST OF FIGURES

Figure 1-1: Surface, double bounce and volume scattering.....	3
Figure 1-2: Polarization Ellipse: major axis (a), minor axis (b), net electric field vector (E), horizontal or propagation axis (x), vertical axis (y)	4
Figure 1-3: Circular Polarization	5
Figure 2-1: (a) Linearly Polarized Wave (b) Elliptically Polarized Wave (c) Circularly Polarized Wave	12
Figure 3-1: In the figure below: a) Vegetation cover map of India (Source: Forest Survey of India). b) Vegetation cover map of Uttarakhand state of India (source: Forest Department of Uttarakhand). c) LISS IV acquired FCC image of Barkot Forest Area. d) Drainage and Compartment map of Barkot Forest.	17
Figure 4-1: Sample Plot.....	21
Figure 4-2: Location of old and new sample plots in the Barkot Forest.....	21
Figure 4-3: Flowchart of Methodology	23
Figure 4-4: Backscatter from upper canopy (σ_{veg0}) and from ground (σ_{gr0}) in WCM.....	34
Figure 4-5 : Backscattering from ground stem interaction (σ_{gs0}) through canopy	35
Figure 4-6: Ground stem interaction through (σ_{gs0}) canopy gaps.....	36
Figure 5-1: (a) Volume scattering image from m-delta decomposition (b) Double bounce scattering from m-delta decomposition.....	38
Figure 5-2: (a) Surface scattering image obtained from m-delta decomposition (b) RGB colour coded image of m-delta decomposition.....	39
Figure 5-3: Contribution of surface, double bounce and odd bounce scattering for every sample plot.	39
Figure 5-4: (a) Volume scattering image obtained from m-chi decomposition (b) Double bounce scattering image obtained from m-chi decomposition.....	40
Figure 5-5: (a) Surface scattering image obtained from m-chi decomposition (b) RGB image obtained from m-chi decomposition.....	40
Figure 5-6: Volume, surface and double bounce scattering obtained after m-chi decomposition from all the sample plots.....	41
Figure 5-7: (a) Volume scattering image obtained from m-alpha decomposition (b) Double bounce scattering image from m-alpha decomposition	42
Figure 5-8: (a) Surface scattering image obtained from m-alpha decomposition (b) RGB colour coded image obtained from m-alpha decomposition	42
Figure 5-9: Scattering information retrieved from m-alpha decomposition.....	43
Figure 5-10: (a) Volume scattering image obtained from Yamaguchi decomposition (b) Double bounce scattering image obtained from Yamaguchi decomposition of Radarsat-2 data.....	43
Figure 5-11: (a) Surface scattering image obtained from Yamaguchi decomposition of fully polarimetric data (b) RGB colour coded image obtained from Yamaguchi decomposition of fully polarimetric data.	44
Figure 5-12: Scattering retrieved from the Yamaguchi decomposition for fully polarimetric data.....	44

Figure 5-13: Comparison of volume scattering with all decomposition methods used in this study.....	45
Figure 5-14: Comparison in double bounce scattering with all decomposition methods used in this study	46
Figure 5-15: Comparison of surface scattering among all decompositions used in this study.....	46
Figure 5-16: (a) Volume scattering obtained using m-delta decomposition against field biomass (b) Volume scattering obtained using m-chi decomposition against field biomass.	47
Figure 5-17: (a) Volume scattering obtained using m-alpha decomposition against field biomass (b) Volume scattering obtained using Yamaguchi decomposition against field biomass.....	47
Figure 5-18: (a) Total backscatter obtained from m-delta decomposition against field measured biomass (b) Total backscatter obtained using m-chi decomposition against field measured biomass.....	48
Figure 5-19: Total backscatter using m-alpha decomposition against field measured biomass (b) Total backscatter obtained using Yamaguchi decomposition against field measured biomass.....	49
Figure 5-20: (a) Modelled AGB using m-delta decomposition against field biomass (b) Modelled AGB using m-delta decomposition against field biomass	51
Figure 5-21: (a) Modelled AGB using m-alpha decomposition against field biomass (b) Modelled AGB using Yamaguchi decomposition against field biomass	51
Figure A-1: The Poincaré Sphere.....	65

LIST OF TABLES

Table 5-1. Estimated β for AGB modelling.....	50
Table 5-2. RMSE obtained for modelled AGB and field biomass	52
Table 5-3. Percent accuracy for modelled AGB	53

1. INTRODUCTION

Forest is an area densely packed by vegetation which contains trees. Forests play an important role in life cycle of human beings. Land surface acquired by forest on this planet is nearly about 30% of the total land surface [1]. Forest also contributes to two third out of the total leaf area of land plants [2]. Environmental changes that lead to loss of species, climatic pattern change and deforestation occur due to change in forest cover [3]. They regularise the climatic system and have great influence on more than 50% biological diversity of the world and more than 1.5 billion people of the world are dependent on forest or forest yield either directly or indirectly [4]. For people in rural area the only source of energy is often fulfilled by burning wood. In Europe and North America, the prime source for heating used by 90 million people is wood energy obtained from forests. For fulfilling their needs like energy, shelter, employment and food, millions of people use these forest outputs. Chao informed that 20% of world population is dependent on forest. Forest and their yields directly and indirectly provide shelter to the world's 18% population [5].

As continuously seen from the last three centuries due to enlargement of agricultural and urban land, more than half of the total forests in the world lost their identity. From the past decades, the rate of deforestation has decreased but in many parts it is still high. Advancement in technology and modernization affect the forest as the forest land is acquired by agricultural land, infrastructure development and cutting of trees for industrial and other purposes. So forest become under scourge today. Forest inventories are used to gather information about forest and its characteristics. This needs constant monitoring of the forests and its characteristics like biomass and stem volume due to its ever changing nature. Two techniques *in-situ* sampling and Remote Sensing are able to derive the changes in the forest. In-situ measurement is laborious and time consuming but more accurate. Conducting field inventory becomes complicated in the heterogeneous forest.

Biomass is the total quantity of living organic matter above the ground, present in trees [2]. Santoro et al., in [6] defined biomass as the material of the plant that is being produced under the photosynthesis reaction. Biomass can also be defined as the volume contained by the forest habitat. Biomass can also be defined as weight of living plant per unit area. Biomass is grouped as Aboveground biomass (AGB) and Below Ground Biomass. Above ground biomass is that quantity of living organic matter of the trees which are present above the ground. AGB is the organic material contained by the living plant above ground excluding root [3]. So above ground biomass contain woods, leaves of trees, branches, shrubs and herbs which are growing above the ground. While below ground biomass is that weight of living plant which is present below the ground surface and it contains roots, tubers.

Remote Sensing is preferable in forest monitoring and also in those areas which are inaccessible for field observation due to its high spatio-temporal resolution. Optical remote sensing is capable of providing

radiometric information about canopy or information about the leaf area index. Optical remote sensing has some limitation in detecting the forest structure under cloud or haze due to its shorter wavelength which cannot penetrate through cloud and haze. This limitation is overcome by Radar remote sensing due to its cloud penetrating capability.

1.1. Radar Remote Sensing

Radar is the abbreviation of Radio Detection and Ranging (Radar). During 1939-45, radar remote sensing came into existence and was used to assess the distance between objects such as ships and aircrafts at the time [7]. Radar is an active imaging microwave remote sensing which transmits its own signal in the form of electromagnetic wave. Sensors used in the radar remote sensing utilize wavelengths from 1 mm to 1 m. The three main functions of Radar are

- Transmit own Radio signals towards a scene.
- Receive backscattered energy from the scene.
- Observes time delay (ranging) and strength (Detection) of the backscattered signals.

Radar wavelengths are longer than wavelengths from optical region of the spectrum. This longer wavelength avail the radar waves to penetrate through cloud as well as partially forest canopy layers, soils and snow. Capability of radar remote sensing in context of vegetation or canopy cover [8] are as follows:

- Ability to penetrate canopy thus offer volumetric information about AGB.
- Sensitive to the water content present in the AGB.
- Ability to penetrate cloud which offer cloud and haze free monitoring of forests.
- Also provide multi-angular sensing to estimate AGB.

Information regarding Earth's surface as surface roughness, moisture (dielectric constant) and topography also provided by radar remote sensing as radar measures both amplitude and phase. In the context of target properties, amplitude rely on dielectric and structure properties while phase rely on the distance between target and sensor. The microwaves scattered from an object basically depends on emissivity and temperature of that object. Emissivity is related to the structure of that object and also content of moisture present in the object. So the scattering retrieved from the object primarily influenced by dielectric constant, texture and polarization. In the case of forest mapping and monitoring, vital role is played by structure of the canopy cover. Retrieved scattering from microwaves are sensitive to the structure and dielectric constant of the trees not for the chemical composition of leaves. A vegetation canopy constituted a complex, diverse volume that comprise components of different shapes, orientation and sizes. Individually retrieved scattering such as surface scattering, double bounce scattering and volume scattering from the target comprise of scattering from leaves of trees, trunks, branches and stems considered as components (Figure 1-1).

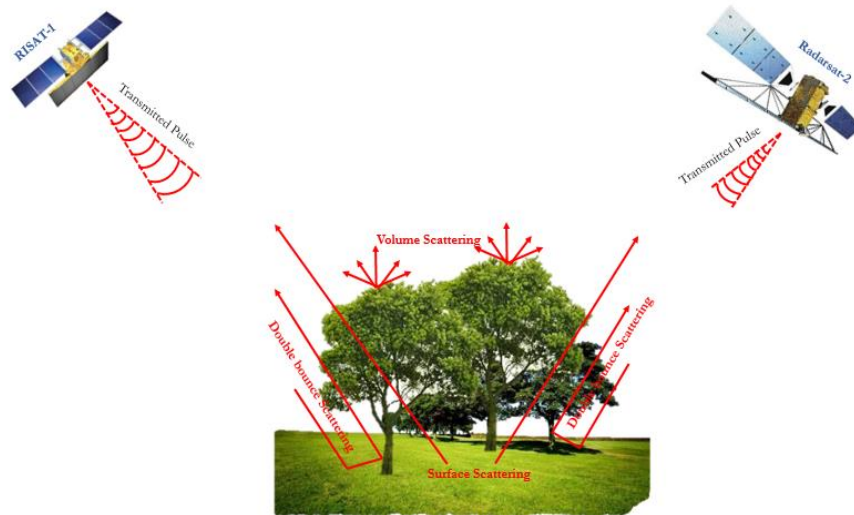


Figure 1-1: Surface, double bounce and volume scattering.

Canopy cover in forests is generally dense and complex so, it can be modelled as volume constituted by randomly oriented objects [7]. Using active remote sensing with the help of microwaves for imaging mode generally advert as radar remote sensing. Synthetic Aperture Radar (SAR) is an application of radar remote sensing.

Synthetic Aperture Radar (SAR) polarimetry is concerned with the utilization of polarimetry in the microwave region of the electromagnetic (EM) spectrum. Polarimetry refers to measure of polarization which is described as the orientation of the electric field vector in a plane perpendicular to the direction of propagation. SAR polarimetry deals with the information retrieval from different scatterers using polarization property of electromagnetic waves. This information from backscatter is in the form of scattering matrix and can be decomposed into covariance and coherency matrices to interpret distributed target which is generated using Pauli's and lexicographic representation [9]. Polarimetric SAR systems have the capacity to separate the contributions of different scattering elements available in single SAR resolution cell. Most used scattering elements for forest studies are surface scattering, volume scattering and double bounce scattering; Incoherent decomposition model was introduced by Freeman and Durden [10] for the decomposition of these surface, volume and double bounce scattering from the targets. Polarization states for SAR are single polarized, dual polarized, quad polarized and hybrid polarized described by the ellipticity (χ) and the orientation angle (Ψ) for polarization also called Polarization Orientation Angle (POA). POA is the angle between the major axis (a) of the polarization ellipse (purple coloured ellipse) (Figure 1-2) of the electromagnetic wave and the horizontal axis in azimuth direction of the moving platform [11]. Shift in orientation angle is brought about by terrain slope as a function of radar look angle and range slope. Shift in POA affects the identification of forest canopy cover. POA is one of the most important characteristics

of the electromagnetic wave which gets disturbed due to scattering from geometrical structures which are haphazardly oriented like forest cover, undulating surface and buildings [11].

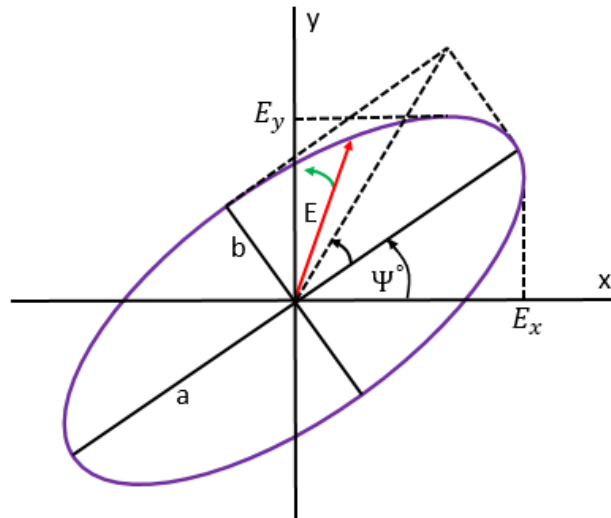


Figure 1-2: Polarization Ellipse: major axis (a), minor axis (b), net electric field vector (E), horizontal or propagation axis (x), vertical axis (y)

Hybrid polarimetry transmit circularly polarized wave (Figure 1-3) and receive two orthogonal mutually coherent polarization [12]. The wave is circularly transmitted linearly received (CTLR). The combination of transmit and receive is as: Right Circular Transmit and Horizontal Received (RH), Right Circular Transmit and Vertical Received (RV), Left Circular Transmit and Horizontal Received (LH) and Left Circular Transmit and Vertical Received (LV) [12] [13]. Another aspect of imaging modes of hybrid polarization is $\pi/4$ mode, the possibility of incorporating data into a polarimetric scattering model. These polarimetric scattering models under some conditions are able to generate the Pseudo-quad-pol information from dual pol mode data [13]. In circularly transmitted wave the polarization orientation angle shift is zero as rotational symmetry is followed by circular polarized electromagnetic waves [14]. Polarization orientation angle shift affects the polarimetric radar signatures and shows overestimation of volume scattering and underestimation of double bounce scattering after decomposition of forest parameters like stem volume and biomass and can be recover by deorientation [15] [16] [17].

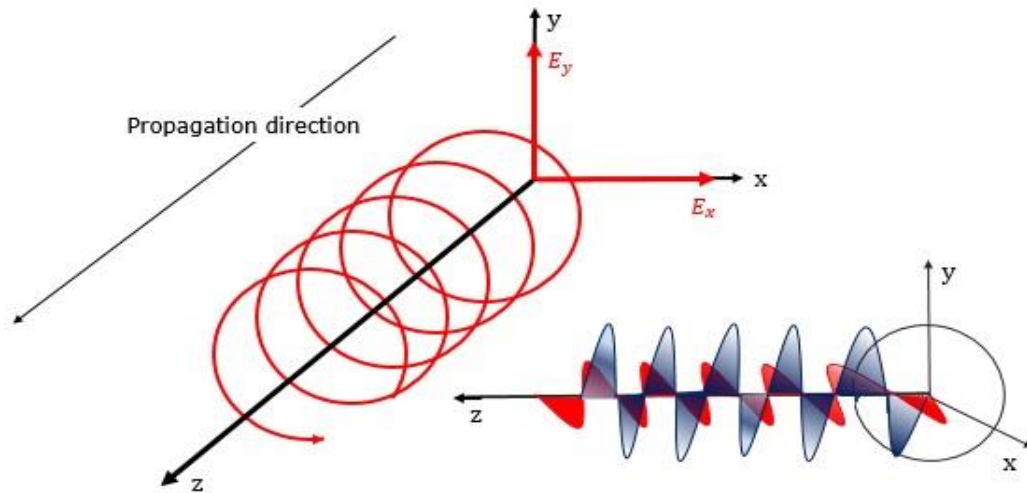


Figure 1-3: Circular Polarization

1.2. Problem Statement and Motivation

PolSAR has already proven its potential for the AGB estimation [18] [19] [20]. PolSAR systems have the capacity to separate the contributions of scattering element in a single SAR resolution cell. Scattering elements obtained from the resolution cell are surface, double bounce and volume scattering. Studies have shown volume scattering is an important parameter for forest biophysical characterisation [21]. It has been observed that random orientation of forest structure causes shift in orientation angle of polarization ellipse. POA changes due to scattering from geometrical structure of topographic slopes, oriented urban area and randomly oriented features like vegetation cover. POA shift affects the polarimetric radar signature and shows overestimation of volume scattering and underestimation of even bounce or double bounce scattering after decomposition [15] [22] [17]. In fully polarimetry and compact polarimetry, transmitted waves contains linear constituents which leads to ambiguities in double bounce scattering. Obtaining a decomposed coherency matrix after POA shift removal using deorientation is a long process. It involves generation of scattering matrix, coherency matrix from scattering matrix, calculating orientation angle from coherency matrix and then performing deorientation on the decomposed coherency matrix is a time consuming and tedious task. Solution to this problem is transmission of wave in circularly polarized manner which produces backscattering that is rotationally invariant. This rotational symmetry is followed by circularly polarized electromagnetic (EM) waves. Hybrid polarimetry (Hybrid Pol) has the advantage of circular transmit and linear receive (CTLR) nature of microwave [12], hence it is unaffected by POA shift. This provides us with a ripe opportunity to use Hybrid PolSAR data to identify contribution to total backscatter from different scatterers for the estimation of AGB using semi-empirical modelling approach.

Aim of this research is retrieval of AGB from Hybrid PolSAR using semi-empirical modelling and validation of modelled AGB with field data as well as from fully PolSAR data. This study could be useful for the regular monitoring of forest where *in-situ* measurement is laborious and time consuming task.

1.3. Research Identification

The present study focuses to estimate the aboveground biomass and potential of Hybrid PolSAR decomposition modelling with the help of Hybrid PolSAR data of RISAT-1. The estimation process admits Extended Water Cloud Model (EWCM) for modelling of forest area. The Barkot forest range is selected to evaluate the strength of Hybrid PolSAR for Aboveground biomass.

1.3.1. Main Objective

The main objective of this research is to evaluate the potential of Hybrid PolSAR data for decomposition modelling and Aboveground Biomass estimation.

1.3.2. Sub-Objectives

- To retrieve the scattering element from Hybrid PolSAR data and fully polarimetric SAR data.
- To compare the decomposition based modelled output for surface double bounce and volume scattering using fully polarimetric SAR and Hybrid PolSAR.
- To estimate the AGB using semi-empirical modelling with Hybrid PolSAR and fully polarimetric SAR data.
- To compare the semi-empirical modelled output with field data as well as with previous studies.

1.4. Research Questions

The following are the research questions identified from the research objectives for the proposed work:

- What will be the significance of Stokes parameters for scattering element retrieval using Hybrid PolSAR data?
- Which decomposition techniques can be used for retrieval of surface, double bounce, and volume scattering information using Hybrid PolSAR data?
- How to retrieve semi-empirical modelling parameters from Hybrid PolSAR data for AGB estimation?
- To what extent the scattering information retrieved from Hybrid PolSAR differ from fully PolSAR?
- How viable is the Hybrid PolSAR techniques for the estimation of AGB in comparison to the results obtained from fully PolSAR based AGB estimation and field data?

1.5. Innovation Aimed At

The key innovation of the current research is at hybrid polarimetry based semi-empirical modelling for forest aboveground biomass using Radar Imaging Satellite-1 (RISAT-1) sensor.

1.6. Structure of the thesis

This thesis describes the decomposition modelling for Hybrid PolSAR data using SAR backscatter. This SAR backscatter is used for retrieving the parameter to estimate the aboveground biomass. Chapter 1 describes about the formulated main objectives and research questions. Chapter 2 is a review of decomposition modelling and different techniques used for the estimation of AGB. Chapter 3 is a detailed explanation of study area. Adopted methodology is described in the chapter 4 with the explanation of data sets and decomposition modelling approaches. Modelling approaches for AGB estimation are described in Chapter 5. Chapter 6 deals with the results obtained using Hybrid PolSAR decomposition modelling and modelling of AGB. Chapter 7 is deals with the discussion of obtained results. Conclusion and recommendations are mentioned in Chapter 8.

2. LITERATURE REVIEW

2.1. Sampling plan for AGB Estimation

There are two techniques which are helpful for biomass estimation: destructive and non-destructive sampling technique. Destructive sampling involves the chopping of the trees and separating out the woody parts and then evaluate the total weight. So it makes this technique laborious, time consuming and also destroy the growth of the trees. Destructive sampling provides the accurate result to estimate the biomass but harvest the whole forest so practically not good. Kumar [3] mentioned that *In-situ* measurements using non-destructive sampling technique is good for biomass estimation because chopping of trees are not required in this process. Regression equations are used which include different parameters in this non-destructive sampling technique. Kangas and Maltamo [23] described the way for sampling to estimate biomass and the sampling designs are given below:

i. Simple Random Sampling (SRS)

This sampling technique involves sampling units containing the samples which are selected by some random process from the whole forest area or population without separating it as homogeneous blocks. SRS is grouped as without and with replacement of sampling unit. In SRS, n-sampling units designed in such a way from the population that equal probability of selecting these sampling units with all possible combinations. The forest area under SRS is considered as a single population. Sample selection that are grouped as without or with replacement worked as the selection of same sample unit is possible only at once and more than once respectively.

ii. Systematic Sampling

Systematic sampling categorized under the non-random sampling where selection of sampling units based upon the predefined pattern. Pattern of these selected sampling units followed thoroughly by regular intervals.

iii. Cluster Sampling

It is described as sample where sampling unit is considered as a group or cluster of elements are known as cluster sample. Husch *et al.*, in [24] mentioned that to form a sampling unit, smaller recording unit or subplots grouped together inside a cluster. Sampling unit is formed by the group of these subplots. Clusters configuration depends on geometric distribution, number of sub plots, distance between units. Cluster sampling is used in large areas such as regional or national inventories. This sampling technique also categorized as single stage and two stage.

iv. Stratified Sampling

Breaking down of a heterogeneous forest into subdivisions through stratification called strata. Stratified Random Sampling involves the division of population into sub populations which are of different strata and then selection of sampling of sampling unit is performed from each of these sub population in proportion to their size. This sampling technique is widely used when heterogeneity in the forest is substantial.

v. Multiphase Sampling

Husch *et al.*, in [25] described this sampling method also as double sampling. This method includes two phases and one variable is determined by using its relationship to another. When obtaining information related to the principal variable makes it costly and difficult in comparison to the other variable than this method is of more interest. Double sampling/Multiphase sampling look for precise estimate by reducing the count of measurements for the costly variable.

2.2. Role of Remote Sensing for the Estimation of AGB

Wulder *et al.*, in [26] applied three approaches using remote sensing data and forest inventory to estimate the biomass. These approaches to estimate the biomass using forest inventory, remotely sensed outputs and hybrid approach. Hybrid approach uses the integration of biomass estimation through forest inventory and remotely sensed outputs methods. Using forest inventory, biomass estimation involves two approaches when developing a model. These are Individual Cover Type (ICT) models and All Cover Type (ACT) models which were based on regression relationships and a single regression relationship respectively between biomass measurements and total volume estimates. In the second and third method remotely sensed data of Landsat TM and hybrid approach respectively used for biomass estimation. Hybrid approach is basically used Polygon Decomposition method. AGB estimates from remote sensing data was 5% lower than the forest inventory. Also there was positive relationship between estimates of AGB of the field and inventory compared to AGB estimation through remote sensing data and field. Study shows that the outcomes of remote sensing approach and forest inventory was varied by 2% in the total estimation of AGB.

2.2.1. AGB Estimation using Active Remote Sensing

Active remote sensing is the technique where transmitted radiation is artificially generated. Active Remote Sensing played a wide role in the estimation of biomass. With the help of Lidar and SAR data above ground biomass is estimated more reliably.

2.2.1.1. AGB Estimation through Lidar

Lidar is the abbreviation of Light Detection and Ranging. In Lidar, laser transmits short pulses of coherent light in a series fashion with a very narrow beam width in a narrow spectral band. Time delay of pulse is used to calculate the distance between the Lidar sensor and the reflecting surface. When Lidar is operated over a forest, first reflection comes out from upper canopy level. But some beams passes through upper canopy and gives reflections from lower canopy and under storey. Final reflection comes from the ground surface [8].

Tree height, which is an important parameter for AGB estimation using volumetric equations was a challenge to extract until the Lidar technology came. Lidar technology is capable to extract the tree height with higher accuracy than other techniques used in remote sensing [27]

Lu *et al.*, in [28] focused on the methods used for above ground biomass estimation using Lidar and Landsat data and analyses that the number of sample plots, suitable algorithms, suitable metrics, and suitable

methods for analyzing uncertainty are the critical issues for the estimation of biomass. Based on the study researchers found that in the estimation of biomass some methods such as sample plots, allometric equations, applied modelling algorithms and spectral variable selection affects the results. Main purpose of Lidar in general is to estimate the canopy height that is also an important variable for tree stand parameters. Challenges faced during the process of mapping biomass in combining the multiscale images, matching sample plot data with images having inconsistent spatial resolution. Three case studies performed by the researchers and found that co-simulation algorithm was helpful for mapping AGB.

Jochem *et al.*, in [29] estimated AGB using semi-empirical model. Then this model was explored for the derived parameters from Airborne Lidar up to canopy transparency level. These parameters used to look into the model for AGB estimation and depend on how much Lidar penetrates the vegetation. Study area used in this study contains alpine forest of area 560 km². In this study semi-empirical model developed by Hollaus *et al.* [29] inquired about its liableness for this forest area. The result of the study showed that semi-empirical model related to stem volume can also be employed for AGB estimation. There is no effect of extended model using different canopy transparency parameters on R².

Tanase *et al.*, in [30] studied the effect on forest biomass estimation using high spatial resolution provided by both Radar and Lidar based Sensors. This study suggests that high-spatial-resolution radar data could provide fundamentally similar results to Lidar for some biomass intervals. Tanase *et al.*, in [30] evaluated the error in biomass retrieval using L-band SAR and Lidar sensors. Study showed that relative error from Lidar based is 9% lower than radar based models for the biomass range of 30-100 t/ha. The author concluded that results provided by radar data and Lidar data at high-spatial resolution are similar for biomass estimation.

2.2.1.2. AGB Estimation through SAR

Hensley *et al.*, in [31] proposed an error model which is derived from backscattering of radar polarimetry for biomass estimates. In this study researchers described the accuracy of estimated biomass assessed from polarimetric radar by using a mathematical framework. Main focus of study was to establish the translation of error that occur due to parametric backscatter measurement to error occurred in biomass estimates. Additionally, researchers also described how the accuracies of expected biomass transformed into design parameters of radar.

Sandberg *et al.*, in [32] estimated the change in forest biomass using P-Band SAR backscatter. Using the reference biomass change maps derived from high density laser scanning data regression models based on backscatter change were developed. The models were selected based on twofold cross-validation technique. The results of the study indicate that the root mean square error of biomass change estimation based on airborne P-band SAR backscatter data is very low. Effects of reduced resolution, increased system noise and ambiguities were simulated when moving from airborne to space borne SAR. The biomass change estimation error was found to be higher when no backscatter offset correction was used. They finally concluded that there is a strong potential for biomass change estimation using P-band SAR backscatter.

Pope *et al.*, in [33] analyzed on the SAR imagery of forest, wetland and agricultural ecosystems of Central America. They developed a four-level landscape hierarchy based upon clustering analysis of the index parameters. They have found that Biomass Index (BMI) was important for differentiating between vegetated and non-vegetated areas and between sloping and level terrain. They have also found that most of the SARs used in the study were single channeled systems and provided only a limited capability for characterizing biomass and structure of tropical vegetation.

Englhart *et al.*, in [18] studied aboveground biomass retrieval in tropical forests using a combination of X and L band SAR data. Two types of datasets of different frequencies i.e. X-band dataset of TerraSAR-X and L-band dataset of ALOS PALSAR were utilized. Calibration of SAR backscatter images were performed using Lidar data. X-band data was found to be efficient for estimation of AGB in area containing low biomass, whereas L-band data effectively derived AGB in area of high biomass. It was also concluded that multi-temporal analysis was more accurate than single-date analysis.

Tanase *et al.*, in [34] adopted a methodology to estimate AGB using multi-temporal L-band data. Biomass maps generated with the help of Lidar data were used as reference maps. Parametric and non-parametric models were used. Backscatter images were generated and polarimetric decompositions were obtained. Hence, effect of polarization on biomass was determined.

The comparative analysis of hybrid-pol data and quad-pol data was conducted by Panigrahi and Mishra [35]. For the accurate comparison hybrid-pol data was first converted into pseudo quad-pol data. Then, decomposition technique i.e. Freeman Durden decomposition was applied to both the datasets. The scattering information retrieved from the decomposition of the images were used as a basis for comparison. It was observed that from hybrid-pol data less scattering information was extracted than the quad-pol data.

2.3. Use of SAR Polarimetry in AGB Estimation

Polarimetry refers to measure of polarization which is described as the orientation of the electric field vector in a plane perpendicular to the direction of propagation. SAR systems transmit polarized EM waves and received these waves as retrieved information from the scatterers also depends on polarization of the transmit wave.

Transmitted and received polarization of complex SAR system are designed as:

- Horizontally transmitted and Horizontally received – (HH)
- Horizontally transmitted and Vertically received – (HV)
- Vertically transmitted and Horizontally received – (VH)
- Vertically transmitted and Vertically received – (VV)

The transmit and receive signal in the above mentioned polarization of SAR systems are categorized as single, dual and quad polarized. Single polarized systems are those whose transmit and receive are either HH or HV or VH or VV. Dual polarized systems are those whose transmit and receive are either HH and

HV or HH and VV or HH and VH. SAR systems which transmit and receive all polarization (HH, HV, VH and VV) are known as quad-polarized.

Another mode of polarization of SAR signal is compact polarimetry. Souyris *et al.*, in [36] introduced the concept of $\pi/4$ compact polarimetry. Compact polarimetry uses the transmitted signal has a single polarization either linear (H+V) at an orientation angle of $\pi/4$ or right circular or left circular with an ellipticity of $\pm 45^\circ$. On the basis of angle of orientation and ellipticity Ferro-Famil and Pottier [37] introduced the conceptual idea of linearly polarized wave or linear polarization, elliptically polarized wave or elliptical polarization and circularly polarized wave or circular polarization.

Figure 2.1 (a), (b) and (c) shows the linearly polarized wave, elliptically polarized wave and circularly polarized wave respectively. E_x and E_y show the horizontal and vertical component of electric field. Red arrow represents the net electric field vector. Green arrow represents the rotation of the net electric field vector. Blue coloured components represents the locus covered by tip of net electric field vector orthogonal to the direction of propagation.

Fully polarimetric data and dual-polarimetric data were analysed by Souissi *et al.*, in [38] compact PolSAR data contains full quad-Pol data and pseudo quad-Pol data. Coherency matrix of compact polarimetric data was used to produce quad-Pol data to reproduce back full quad-Pol data. The two datasets were subjected to Yamaguchi decomposition and the results were examined. Compact PolSAR data was observed to be less efficient than the fully polarimetric data. Full polarimetric data (FP) generated 4×4 coherency matrix whereas compact polarimetric data generated 2×2 coherency matrix.

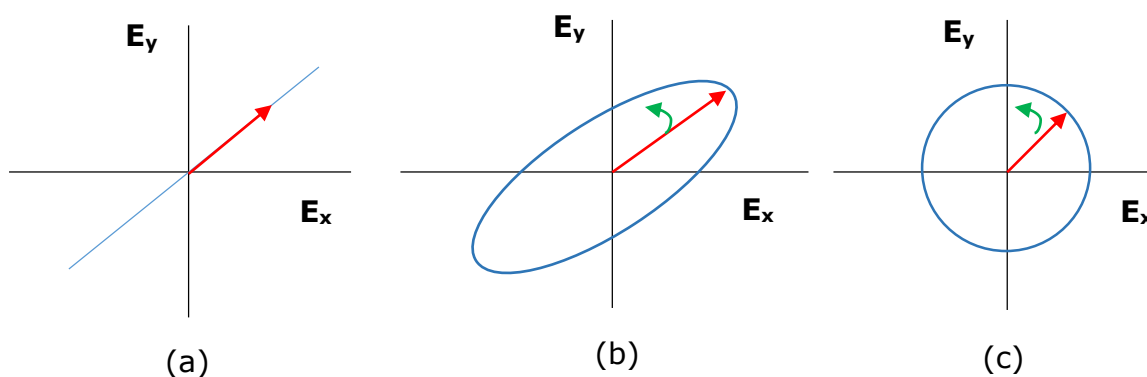


Figure 2-1: (a) Linearly Polarized Wave (b) Elliptically Polarized Wave (c) Circularly Polarized Wave

2.4. Hybrid Polarimetry

Hybrid polarimetry has the advantage over other polarimetry as it can transmit circularly polarized wave and receive two orthogonal mutually coherent polarizations [12]. The wave is circularly transmitted linearly received (CTLR). The combination of transmitted and received signal is as: Right Circular transmit and Horizontal received (RH), Right Circular transmit or Vertical received (RV) [12].

Raney [12] show that circularly polarized light is transmitted and linearly polarized light is received in Hybrid-Polarity architecture (CL-pol) of SAR which is a reflexion of compact polarimetry. Study showed that resulting radar has low susceptibility for cross channel errors and noise. Study concluded that measure of amplitude of backscatter and relative phase is required for Stokes parameter and the values of Stokes parameter are also free from polarization basis. Raney [14] concluded that if transmitted signal is circularly polarized then only elements of Stokes vector are rotationally invariant. CTLR with relative phase are sufficient for the retrieval of Stokes parameter. The advantage of system calibrations with relative phase and gain are provided by Hybrid polarity architecture.

2.5. Polarimetric decomposition for the estimation of AGB

Polarimetric decomposition is the technique of discriminating individual scattering from targets. This leads to better interpretation of target on the ground. Geometric and physical properties of the target can be retrieved by polarimetric decomposition. Decomposition techniques categorized as coherent decomposition and incoherent decomposition. Coherent decomposition is addressed by scattering matrix and well fitted for pure targets and these are named after Pauli, Cameron and Kroagager [39] [40]. The incoherent decomposition addressed by coherency matrix or covariance matrix obtained from target vectors [10] [41]. Incoherent decomposition is well suited for the AGB as partially polarized wave (neither perfectly Horizontal nor Vertical but rather a sum of both) is scattered by natural objects as they are distributed (randomly oriented) targets.

A simple model was developed by [42] for microwave backscattering of vegetation canopy. This model employed earth surface as constituting of two-layers, vegetation and ground. Vector Radiative Transfer model is applied for modelling of backscattering information retrieved from vegetation.

Freeman and Durden [10] proposed a three component scattering model for polarimetric decomposition of SAR data. It involves three scattering mechanisms. These scattering are canopy scattering from upper layer of vegetation or from randomly orientated dipoles, double bounce scattering from corner reflectors, Bragg scattering from rough surface. Freeman-Durden decomposition work is extended by [43] for PolInSAR data sets. Magnitude and phase has defined parameters retrieved from PolInSAR. In this study new features got identified as a result from both PolSAR and PolInSAR data.

Recognition algorithm developed by [44] by applying Kroagager polarimetric decomposition for Automatic Target Recognition (ATR) of either man-made or natural target by using one or more fully polarimetric SAR imagery.

Jayasri et al. (2013) presented a paper on m-delta decomposition of hybrid dual polarimetric SAR data of RISAT-1. They concluded that the power scattered by even bounce and odd bounce targets are dependent on the state of polarization and relative phase value of the targets. Turkar et al. (2012) observed that by using m-delta and m-chi decomposition along with circular polarization ratio (CPR) and SPAN of hybrid polarimetric data, land cover classification accuracy can be improved.

2.6. Model Based Measurement to Estimate the AGB

Attema and Ulaby [47] proposed a model to calculate the biomass in which vegetation modeled as a water cloud. This model was named as WCM. The proposed model considers canopy as a water cloud and droplets of this water cloud considered as vegetative matter. Developed model assume water droplets indistinguishable under the canopy cloud which are haphazardly distributed among the canopy. Backscattering coefficient derived in this model based on target parameters which are three in numbers. These target parameters are height of the plant, volumetric moisture and water content of soil and vegetation respectively. These parameters were assessed by radar cross section data using regression analysis. WCM was extended by Liu *et al.*, in [48] to a Two Layer Water Cloud Model (WCM2). WCM considers canopy as homogeneous medium and ignores heterogeneity in vegetation layer. In the WCM2 vertical heterogeneity is taken into account. This heterogeneity of vegetation accounted by distributing per unit volume water content. Validation of the results performed with the Tor Vergata model which is a physical model [49].

Zhou and Hamstrom [50] made a comparative study in order to estimate the AGB. They concluded that the Jenkins and the Component Ratio Methods (CRM) estimate the higher merchantable biomass when comparing with the estimates of the regionally derived equations. The Jenkins model was designed for national level biomass estimation [51]. It uses a set of equation for the estimation of total above ground biomass based on the diameter of a tree. The Jenkins model is a more generalized approach and the results might be misleading when applied at fine scales. The CRM method is a refinement to the Jenkins method and may alleviate consistency problems associated with the regional equations.

Kumar et al., in [52] applied a genetic algorithm on the estimation of water cloud model vegetation parameters. They considered four parameters: two parameters to characterize the vegetated terrain and the other two were for the bare soil parameters. The vegetation parameters were estimated using a Genetic Algorithm optimization technique. The results of the study demonstrated that the Genetic Algorithms are superior over conventional methods of optimization provides confidence in its use for estimation of hydrological parameters from other SAR images.

Englhart *et al.*, in [53] compared three techniques for AGB estimation. Multi-frequency SAR data i.e. TerraSAR-X and ALOS PALSAR was employed in the study. Lidar data was utilized as reference data. The three algorithms used were multivariate linear regression (MLR), artificial neural network (ANN) and support vector regression (SVR). The ANN and SVR models resulted in higher coefficients of determination and higher error measures when compared to the MLR model. The MLR showed overestimation of biomass range.

Sandberg *et al.*, in [32] develop different regression models and the models were compared to the change maps based on laser data using two-fold cross-validation and estimation error were also evaluated. The results of the study indicates that the root mean square error of biomass change estimates based on P-band SAR backscatter is 15% or 20% t/ha.

Jochem *et al.*, in [29] used a semi-empirical model that was originally generated for stem volume estimation is used for AGB estimation of a spruce dominated alpine forest. The study shows that the introduction of canopy transparency parameters does not change the results significantly according to coefficient of determination in comparison to the results derived from the semi-empirical model which was originally developed for stem volume estimation.

Poolla [22] used extended Water Cloud Model in which higher order interaction (stem-ground interaction) was considered. In this extended water cloud model double bounce scattering taken into account by using L-band data that occur due to stem-ground interaction. This study showed that volume scattering has reduced and double bounce scattering has increased after deorientation. With the increase in above ground biomass, volume scattering also increases up to certain value after that saturation occurs. There was no equal relationship between decrease in volume scattering and increase in surface scattering. Determination coefficient before and after the deorientation of stem volume was 0.315 with RMSE of 328 m³/ha and 0.4259 with RMSE of 185 m³/ha respectively. The result of the extended water cloud model provide reliable accuracy after deorientation for the estimation of AGB.

Kumar *et al.*, [20] studied on the estimation of AGB using C-band data of ENVISAT for a tropical forest. The forest parameters were obtained using semi-empirical modelling i.e. WCM and Interferometric Water Cloud Model (IWCM) through the use of SAR backscatter and Interferometric Synthetic Aperture Radar (InSAR) coherence. The study achieved high AGB accuracy with low root mean square error based weighting coefficients and WCM multi-data and InSAR images showed better results compared to individual coherence images.

3. STUDY AREA

To study the potential of Hybrid PolSAR for aboveground biomass, a site is chosen in Barkot Forest. Barkot Forest has diverse trees structures due to various tree species present in it. Due to this diversity, the retrieved scattering has all the component (surface scattering, volume scattering and double bounce scattering) which will be required in decomposition modelling. The forest has a major contribution in the volume scattering.

3.1. Introduction

The Barkot Forest is situated at the foothills of Himalaya in the Uttarakhand state of Northern India. Location of the forest area lies in between 29°33' to 30°00' N latitude and 78°18' to 79°49' E longitude. The Barkot Forest is located between Gharwal and Shivalik ranges of the Himalayas and also bordered by the city Rishikesh and the river Ganges. Barkot forest range come under west gangetic moist deciduous forest which covers around 1800 km² area [17] [54]. It is a type of closed forest that belongs from medium height trees to good heights. The regeneration status is poor for the Sal trees in this forest. The vegetation type of this forest can be grouped as follows.

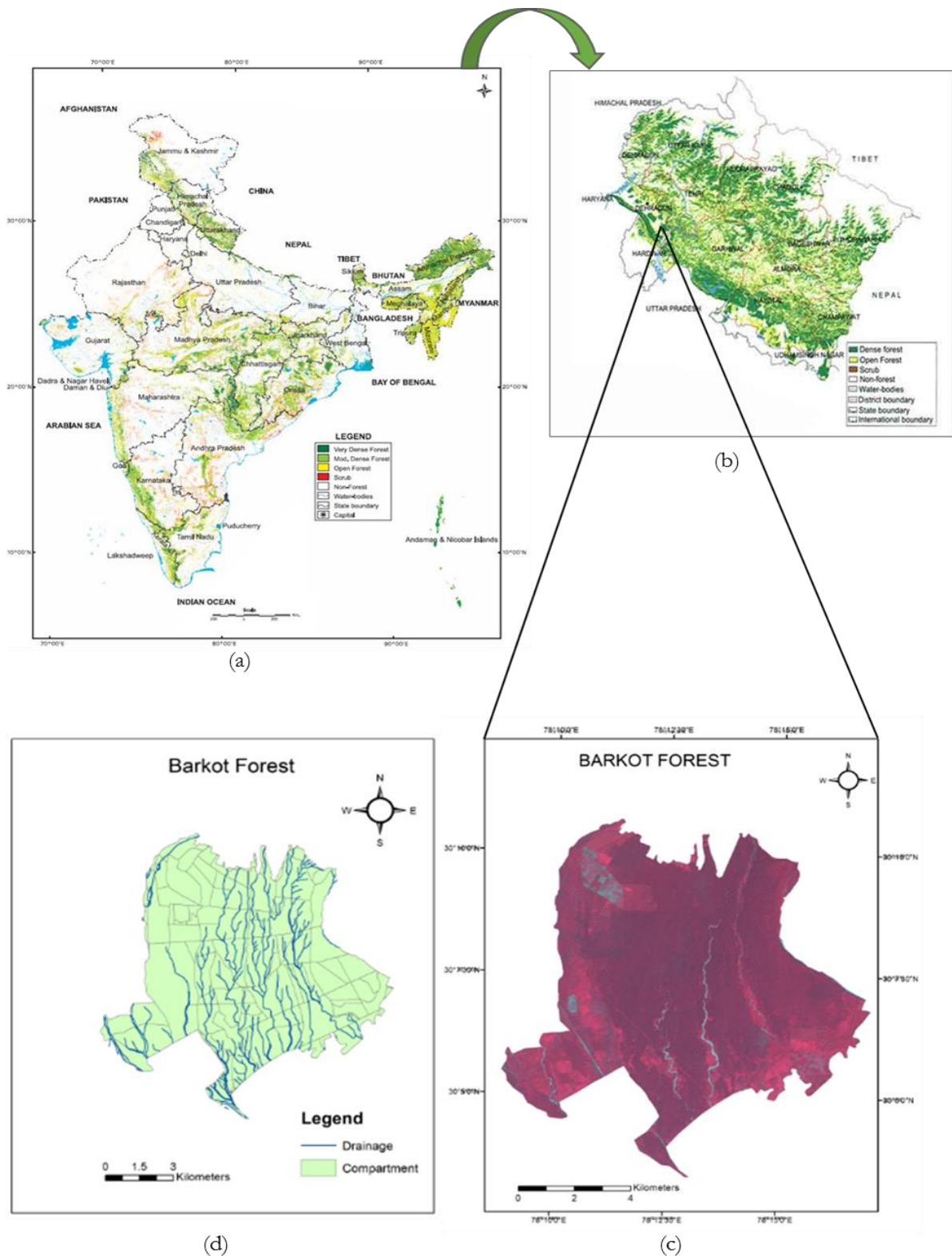
- Sal forest
- Mixed Sal forest
- Teak plantation
- Mixed Teak plantation
- Acacia

Barkot Forest is situated nearby the Rajaji national park with a dense canopy cover of vegetation. Vegetation cover map of India is given in Figure 3.1 (a) while the vegetation cover map of Uttarakhand state of India is given in Figure 3.1 (b). False colour composite (FCC) image acquired by LISS IV sensor of Resourcesat-2 is shown below in Figure 3.1 (c) and drainage pattern map of the same area is given in Figure 3.1 (d).

3.2. Block wise division of Barkot Forest

Barkot forest has been grouped into several blocks according to Forest department of Uttarakhand. The blocks in which Barkot Forest is grouped are as Sainkot, Ranipokhari, Bhaniawala, Jakhan, Ghamandpur, Jogiwala and Chandi.

Figure 3-1: In the figure below: a) Vegetation cover map of India (Source: Forest Survey of India). b) Vegetation cover map of Uttarakhand state of India (source: Forest Department of Uttarakhand). c) LISS IV acquired FCC image of Barkot Forest Area. d) Drainage and Compartment map of Barkot



3.3. Statement of significance

Dense Sal trees has a major share in the Barkot Forest Area which also contributes to the volume scattering from their dense canopies. Seasonal growth in agricultural lands around the forest area also contributes to the volume scattering while at the same time of land without crop this part contributes as surface scattering. Areas having low or no vegetation near or inside forest contribute towards double bounce.

Backscatter from this area is contributed by surface, volume and double bounce scattering, which is needed in this project for decomposition modelling to estimate AGB. No extra effort is need to filter out any bias due to topography as the study area is relatively plain. Hence Barkot Forest was chosen as the study area for this research.

3.4. Climate

The climate of this area is humid with moderate to cold temperature having rainfall and luxuriant vegetation. Different seasons in this area are: summer (March to May), rainy season (May to mid-September) and winter (mid-September to mid-march).

Monsoon: Generally the rainfall starts approximately from May and ends in August at Doon valley. The recorded annual rainfall varies from lower 153.3 cm to higher 287.6 cm. Maximum and minimum rainfall occur during the months of April and July-August respectively.

Temperature: Temperature varies from 21.2° C to 40° C up to the month of May while in the winter it varies in between 5° C to 23° C. Minimum and maximum recorded humidity of this area during April and July are 35.7% and 86% respectively at 8:30 hrs.

3.5. Soil

Soil of this forest consist of clays, sand, stones of small sizes to big sizes, boulders and pebbles. Soil morphology of this area had characteristics from non-sticky friable to sticky firm. Most of the time in year, soil of this forest remains moist due to lessened evaporation up to tree density from floor of the forest and high canopy cover. Organic matter content in the soil are heavy with moderate plant litter. The pH concentration of the soil is 5.64 meaning it is moderately acidic in nature. Texture percentage in this soil for sand, clay and silt are 64.56%, 21.14% and 14.15% respectively (Mukesh et al. 2011). Calcium, magnesium and potassium are the major constituents of soil present in in this forest. Quartz, mica and feldspars were also identified in this forest.

3.6. Flora

The main contribution in this forest area is by Sal (*Shorea robusta*) trees. Sal trees which are dominant species assisted with Teak (*Tectona grandis*), Sisoo (*Dalbergia sisoo*) and Khair (*Senegalia catechu*). Some other trees which also have contribution to this forest are Rohini (*Mallotus philippensis (Lamk) Muell.-Arg.*), Chamror (*Ebretia laevis Roxb.*), Kanju (*Holoptelea integriflora (Roxb.) Planch.*) and Sagaun (*Tectona grandis L.f.*). Safed siris (*Artabotrys odoratissimus*), dhauri (*Anogeissus Pendula*), bohera (*Tamarindus indica*) and jhingan (*Lannea coromandelica*) are also the main companion of Sal. Sal trees have about 40% contribution as dominating species to this forest area. Sal, Khair and sisoo covered northern part of this forest area while mix species like bamboo, grass and shrubs is in the southern part of this forest area.

3.7. Fauna

Wildlife of this forest is quite diverse. This forest has the largest population of Elephants (*Elephas maximus*). The other species of mammals that belongs to this forest are Tigers (*Panthera tigris*), Wild cats, Neelgai (*Boselaphus tragocamelus*), leopards, Deer, Langoons (*Simia entellus*).

4. MATERIALS AND METHODS

This chapter is a detailed description of satellite data and collected field data with the explanation of field estimated AGB for the study area. Chapter also given description of adopted methodology with the description of Hybrid PolSAR decomposition techniques and fully PolSAR decomposition technique that were used for the AGB estimation. Forty five plots were available with their recorded global positioning system (GPS) locations. Four more plots have been collected so the total 49 plots were available. Required information has been extracted in the form of backscatter values from these locations. This information was used to estimate the AGB for these locations.

4.1. Materials

4.1.1. Satellite Data

Two datasets are used in this study. The available datasets were from two different sensors RISAT-1 and Radarsat-2. Both the datasets are in Single Look Complex (SLC) format. The specification of datasets are shown in Table 4-1.

Table 4-1: Description of the available data.

Description	Image 1	Image 2
Satellite	RISAT-1	RADARSAT-2
Date of Acquisition	01-July-2013	28-Jan-2014
Band	C	C
Polarization	Hybrid Pol	Quad Pol
Data Format	SLC	SLC
Mode	FRS-1	Fine Quad Pol
Wavelength	5.6 cm	5.5 cm
Resolution	2.34 m × 3.33 m	5.2 m × 7.7 m

Transmission mode of available data of RISAT-1 is in right circular transmit mode.

4.1.2. Field Data

There were 45 plots collected in a previous research [17]. Four more plots have been collected in Barkot forest range so the total 49 plots were available. During the month of December, fieldwork has been carried out to collect four more sample plots. Newly collected sample plots were from Sal forest and mixed Sal forest. Plots were collected using stratified random sampling method. The area of collected sample plots were 0.1 ha with square shape (shown in Figure 4-1). Circumference at breast height (CBH) and Diameter

at breast height (DBH) are tree parameters those were collected to estimate the AGB at each plot. The distribution of sample plots are shown in Figure 4-2.

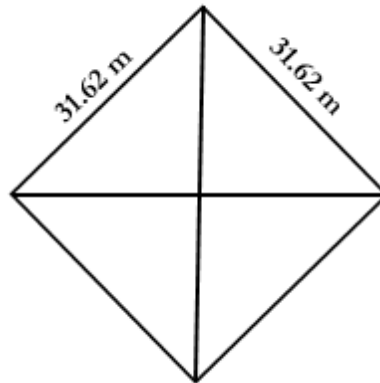


Figure 4-1: Sample Plot

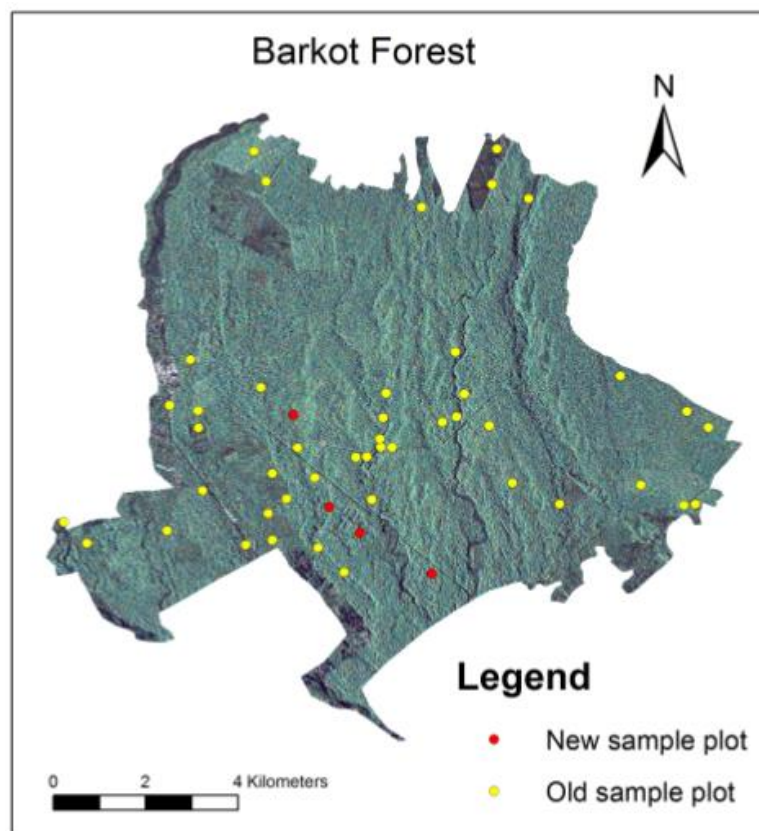


Figure 4-2: Location of old and new sample plots in the Barkot Forest

4.1.3. Calculations of field estimated AGB

Tree parameters which was calculated in the forest used to calculate the AGB. For each tree CBH and height of the tree was measured for every locations. DBH is calculated with the help of CBH. Forest Survey of

India (FSI) has developed stand volume equations. Stand volume has been calculated using these equations. Empirical models developed by FSI [55] for each type of species.

4.1.3.1. Basal Area

For each tree species basal area (A) was calculated with the help of measured stem diameter using the equation (4.1);

$$A = \pi \left(\frac{\text{stem diameter}}{2} \right)^2 \quad (4.1)$$

4.1.3.2. Stem Volume

On the basis of stem volume equation provided by FSI [55] (Appendix A), stem volume was calculated and tree species for which equations are not available, the quarter girth formula is given in equation (4.2);

$$V_{qg} = \pi(r)^2 h \quad (4.2)$$

Where stem volume is represented as V_{qg} , r refers to radius and h refers to tree height.

4.1.3.3. Aboveground Biomass (AGB) estimation

This stem volume (calculated in field) and specific gravity used to calculate the AGB is given in equation (4.3);

$$AGB = SV \times SG \quad (4.3)$$

Where SV refers to stem volume and SG refers to specific gravity. The unit of stem volume (SV) is m^3 . Specific gravity values were taken from Indian Woods book [56]. Empirical models developed by FSI for considering stem volume only included those trees which have stem diameter greater than 10 cm. The four more plots collected in the field are present in Sal forest and mix Sal forest. AGB has been calculated for these plots using basal area and stem volume with the help of field measurements like tree height and CBH. AGB for these 4 plots ranges from 21.42 ($t \text{ ha}^{-1}$) to 282.92 ($t \text{ ha}^{-1}$) with an average AGB of 251.54 ($t \text{ ha}^{-1}$).

4.2. Methodology

Flow diagram of adopted methodology to generate SAR backscatter images and to estimate AGB is given in Figure (4-3);

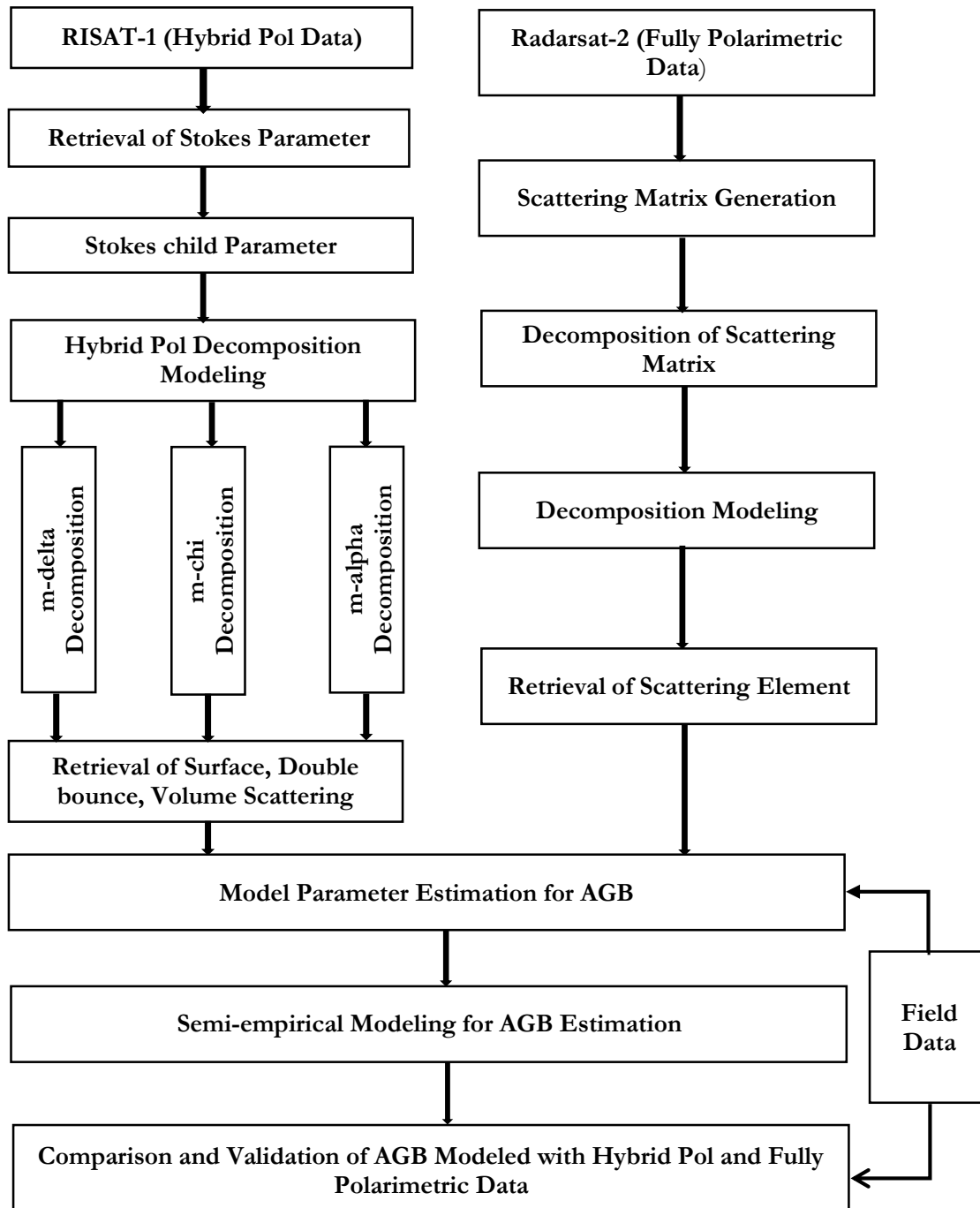


Figure 4-3: Flowchart of Methodology

4.3. Stokes parameters

George Gabriel Stokes has defined that the polarization state of an electromagnetic wave can be expressed by the Stokes parameters. For fully polarized waves the amplitude and relative phase are constants or varying slowly with time. To deal with partially polarized wave it is easier to use Stokes parameters as compared to fully polarized wave. These parameters describe partially polarized waves not by their phases and amplitude but by their observable power terms. Stokes parameters are S_1 , S_2 , S_3 and S_4 . Representation of Stokes parameters have primarily two advantages that all four parameters are measured in terms of their intensities and has the capability to deliver partially polarized waves in the form of 2×2 complex hermitian positive semi-definite wave coherency matrix $[J]$ [57]. This coherency matrix also known as Wolf's coherence matrix [58] and expressed as in equation (4.4):

$$[J] = \langle EE^\dagger \rangle = \begin{bmatrix} \langle E_H E_H^* \rangle & \langle E_H E_V^* \rangle \\ \langle E_V E_H^* \rangle & \langle E_V E_V^* \rangle \end{bmatrix} = \begin{bmatrix} J_{HH} & J_{HV} \\ J_{VH} & J_{VV} \end{bmatrix} = \frac{1}{2} \begin{bmatrix} S_1 + S_2 & S_3 + jS_4 \\ S_3 - jS_4 & S_1 - S_2 \end{bmatrix} \quad (4.4)$$

where E is the complex voltage (in the subscripted polarization), \dagger denotes complex conjugate transpose, $*$ denotes complex conjugate and $\langle \dots \rangle$ indicates ensemble averaging (here multilooking) by assuming wave is stationary [57]. Stokes vector (S) can be associated with the coherency matrix $[J]$ as [57] in equation (4.5)

$$\begin{aligned} S_1 &= \langle |E_H|^2 + |E_V|^2 \rangle = \langle E_H E_H^* \rangle + \langle E_V E_V^* \rangle = J_{HH} + J_{VV} \\ S_2 &= \langle |E_H|^2 - |E_V|^2 \rangle = \langle E_H E_H^* \rangle - \langle E_V E_V^* \rangle = J_{HH} - J_{VV} \\ S_3 &= 2\langle |E_H||E_V| \cos \phi_{HV} \rangle = \langle E_H E_V^* \rangle + \langle E_V E_H^* \rangle = J_{HV} + J_{VH} \\ S_4 &= 2\langle |E_H||E_V| \sin \phi_{HV} \rangle = j\langle E_H E_V^* \rangle - j\langle E_V E_H^* \rangle = jJ_{HV} - jJ_{VH} \end{aligned} \quad (4.5)$$

Since $[J]$ is positive semidefinite matrix so,

$$\det\{[J]\} \geq 0 \text{ or } S_1^2 \geq S_2^2 + S_3^2 + S_4^2 \quad (4.6)$$

In equation (4.4) intensities is represented by diagonal elements while complex cross correlation is shown by off-diagonal elements (between E_H and E_V). Total energy is represented by $\text{Trace}\{[J]\}$.

This study involves RISAT-1 coherent dual-polarized SAR data where the transmitted electromagnetic waves are in right circular mode and sensor is receiving horizontal and vertical polarized waves. So the Stokes parameters in circular and linear polarization at receiver can also be expressed as equation (4.7) [12];

$$S_1 = \langle |E_{RH}|^2 + |E_{RV}|^2 \rangle$$

$$\begin{aligned}
 S_2 &= \langle |E_{RH}|^2 + |E_{RV}|^2 \rangle \\
 S_3 &= 2\text{Re}\langle E_{RH}E_{RV}^* \rangle \\
 S_4 &= -2\text{Im}\langle E_{RH}E_{RV}^* \rangle
 \end{aligned} \tag{4.7}$$

Where E_{RH} and E_{RV} are complex voltage in right circular transmit with horizontal and vertical receive polarization, Re and Im refers to the real and imaginary value respectively obtained from complex cross product. To describe the polarization state on Poincare sphere (Appendix A), the required components are degree of polarization (m), ellipticity parameter (χ) and orientation angle (Ψ). On the basis of these three (m, χ, Ψ) components Stokes vectors can also be expressed as in equation (4.8) [57];

$$S = \begin{bmatrix} S_1 \\ S_2 \\ S_3 \\ S_4 \end{bmatrix} = \begin{bmatrix} S_1 \\ S_1 \cos(2\psi) \cos(2\chi) \\ S_1 \sin(2\psi) \cos(2\chi) \\ S_1 \sin(2\chi) \end{bmatrix} \tag{4.8}$$

From all the four Stokes parameters the only dependent parameter is S_1 while the remaining three parameters are independent. The first parameter S_1 refers to the total intensity of the electromagnetic wave. The second parameter S_2 refers to the polarization state. Parameters S_3 and S_4 respectively refers to rotation and phase difference. The Stokes parameters also accompanied to matrix decomposition techniques.

4.3.1. Stokes Child Parameters

The parameters derived from or with the help of Stokes parameters are known as Stokes child parameters. They are degree of polarization (m), relative phase (δ), ellipticity parameter (χ), polarization angle (α) and circular polarization ratio (μ). All the mentioned child parameter can be described with the help of Stokes parameters as [12];

Degree of Polarization (m): On the Poincaré sphere, the degree of polarization represents the distance of a normalized Stokes vector's last three components from the origin. The surface of the unit Poincaré sphere (Appendix A) corresponds to m equals to one and represents all totally polarized states. In other words m is the representative of polarized and diffuse scattering and can be calculated using Stokes parameters as in equation (4.9);

$$m = \frac{\sqrt{S_2^2 + S_3^2 + S_4^2}}{S_1} \quad 0 \leq m \leq 1 \tag{4.9}$$

Relative Phase (δ): Relative phase is the phase between RH and RV (for this study) and can be calculated using Stokes Parameters as in equation (4.10);

$$\delta = \tan^{-1}\left(\frac{S_4}{S_3}\right) \quad -180^\circ \leq \delta \leq 180^\circ \quad (4.10)$$

Chi (χ): χ is the ellipticity parameter which preserves the sense of rotation when the transmitted field is elliptically polarized. χ enters the decomposition as in equation (4.11);

$$\sin(2\chi) = -\frac{S_4}{mS_1} \quad -45^\circ \leq \chi \leq 45^\circ \quad (4.11)$$

Polarization angle (α): Polarization angle can be calculated using Stokes parameters as;

$$\alpha = \frac{1}{2} \tan^{-1}\left(\frac{\sqrt{S_2^2 + S_3^2}}{S_4}\right) \quad (4.12)$$

Circular Polarization Ratio (μ): Circular polarization ratio is an indicator of planetary ice deposits and also double bounce scattering. It can be calculated using Stokes parameters as in equation (4.13);

$$\mu = \frac{S_1 - S_4}{S_1 + S_4} \quad \mu \geq 0 \quad (4.13)$$

4.3.2. Hybrid PolSAR Decomposition Modelling

Three decomposition model was used for to perform this study for Hybrid PolSAR data. Hybrid Pol decomposition model used in this study was m-delta decomposition, m-chi decomposition and m-alpha decomposition. Backscatter images were generated using these decomposition model to extract the required information in the form of surface, volume and double bounce scattering.

4.3.2.1. m-delta (m- δ) decomposition

The m-delta decomposition comprise of degree of polarization (m) and relative phase (δ). Raney *et al.*, in [12] introduced the practical applicability of (m- δ) decomposition. The parameters used for this modelling approach basically derived from the Stokes parameter. Degree of polarization (DoP) is indicating polarized and diffuse scattering. Relative phase (here phase between RH and RV) is indicating double bounce scattering. DoP and relative phase are able to characterize the polarization state of electromagnetic wave and can be expressed with the help of Stokes parameters [14] as given in equation (4.9) and equation (4.10).

The value of degree of polarization lies in between 0 to 1 ($0 \leq m \leq 1$) where $m = 1$ represents the totally polarized wave. While the value of relative phase lies in between -180° to $+180^\circ$ ($-180^\circ \leq \delta \leq +180^\circ$) where $-$ and $+$ sign of the relative phase represents rotation direction of

circularly polarized field [45]. The negative phase indicate rotation direction is right circular while the positive phase indicate the left circular rotation. The $(m-\delta)$ can be expressed as in equation (4.14) to (4.16)

$$f_{odd(m-\delta)} = \sqrt{s_1 \times m \times \frac{1 + \sin(\delta)}{2}} \quad (4.14)$$

$$f_{even(m-\delta)} = \sqrt{s_1 \times m \times \frac{1 - \sin(\delta)}{2}} \quad (4.15)$$

$$f_{volume(m-\delta)} = \sqrt{s_1 \times (1 - m)} \quad (4.16)$$

Where $f_{odd(m-\delta)}$, $f_{even(m-\delta)}$ and $f_{volume(m-\delta)}$ indicates the relative contribution of surface, double bounce and volume scattering respectively retrieved from this decomposition modelling. In this decomposition technique, m is the sensitive indicator of volume scattering and δ is the sensitive indicator of even bounce against odd bounce scattering.

4.3.2.2. m-chi (m- χ) Decomposition

Raney *et al.*, in [59] applied the $(m-\chi)$ decomposition for hybrid polarimetric data. The $(m-\chi)$ decomposition consist of degree of polarization (m) and ellipticity parameter (χ). This decomposition model is using parameters m and χ which are derived from Stokes parameters. The DoP is indicating diffuse scattering while χ is an indicator of even versus odd scattering as the sign of χ is an unambiguous indicator of even versus odd bounce scattering. The value of DoP lies in between 0 to 1 ($0 \leq m \leq 1$) while chi lies in between -45° to $+45^\circ$ ($-45^\circ \leq \delta \leq +45^\circ$). The (χ) enters in this decomposition modelling in the form of degree of circularity [59] as given in equation (4.11).

Using equation (4.9) and equation (4.11) the m-chi decomposed image can be expressed as;

$$f_{odd(m-\chi)} = \sqrt{s_1 \times m \times \frac{1 + \sin(2\chi)}{2}} \quad (4.17)$$

$$f_{even(m-\chi)} = \sqrt{s_1 \times m \times \frac{1 - \sin(2\chi)}{2}} \quad (4.18)$$

$$f_{volume(m-\chi)} = \sqrt{s_1 \times (1 - m)} \quad (4.19)$$

The relative contribution of surface, double bounce and volume scattering are indicated as $f_{odd(m-\chi)}$, $f_{even(m-\chi)}$ and $f_{volume(m-\chi)}$ respectively retrieved from this $m-\chi$ decomposition modelling.

4.3.2.3. m-alpha (m- α) Decomposition

The m-alpha decomposition comprise of DoP (m) and polarization angle (α). This decomposition method is based on Eigenvector analysis of Hybrid PolSAR data and similar to H/ α decomposition of fully polarimetric data [60]. This α parameter can only be estimated from Hybrid PolSAR data when there is dominant scattering from urban and agriculture fields (dominant eigenvector of T3). The α parameter can be expressed with the help of Stokes parameters as given in equation (4.12). The α parameter represents the scattering mechanism.

Unit of α parameter is in degree and also closely related to the ellipticity of the compact scattered wave as [61];

$$\alpha = 2|\chi|$$

Using equation (4.9) and equation (4.12) the m-alpha decompose imaged can be expressed with the help of Stokes parameter, DoP and alpha as equations (4.20) to (4.22) [61];

$$f_{odd(m-\alpha)} = \sqrt{s_1 \times m \times \frac{1 + \cos(2\alpha)}{2}} \quad (4.20)$$

$$f_{even(m-\alpha)} = \sqrt{s_1 \times m \times \frac{1 - \cos(2\alpha)}{2}} \quad (4.21)$$

$$f_{volume(m-\alpha)} = \sqrt{s_1 \times (1 - m)} \quad (4.22)$$

The value of α lies between 0° to 90° ($0^\circ \leq \alpha \leq +90^\circ$). The alpha parameter here is the scattering mechanism. Where $f_{odd(m-\alpha)}$, $f_{even(m-\alpha)}$ and $f_{volume(m-\alpha)}$ indicate the contribution of surface, double bounce and volume scattering respectively retrieved from this m- α decomposition modelling.

4.3.3. Fully PolSAR Data Processing

Fully PolSAR utilizes all the polarization channel (HH, HV, VH and VV). This utilization helps in extracting all the required information (scattering) from a single SAR resolution cell. Before generating scattering matrix pre-processing of data is required. The available data was in SLC format. The available Radarsat-2 data is compressed and in slant range. Multilooking is the process in which square pixels are generated to remove slant-range distortion. To achieve ground range resolution SLC data was multilooked. The number of looks taken in azimuth and range direction are two and one respectively.

4.3.3.1. Generation of Scattering Matrix

When any polarized EM wave interacts with a target, the wave is scattered from that target contain both polarization (horizontal and vertical). The backscattering from target can be described by scattering matrix (SM). Scattering matrix is a 2×2 matrix. As the backscattering from target can be represented by 2×2 matrix so this 2×2 matrix provide the information about target as radar image is dependent on geometry and orientation of target . The scattering matrix can be represented as in equation (4.23);

$$SM = \begin{bmatrix} S_{HH} & S_{HV} \\ S_{VH} & S_{VV} \end{bmatrix} \quad (4.23)$$

Currently there are four elements in the scattering matrix which are complex and can be measured through magnitude and phase from the subscripted polarization channel [62]. If reciprocity condition is assumed ($S_{HV} = S_{VH}$) then four elements of scattering matrix will be reduced to three. Reciprocity condition can only be assumed for monostatic systems and it makes the scattering matrix symmetrical.

Information extraction from scattering matrix is advantageous if the target are coherent target or pure target. Extraction of information from incoherent target like vegetation can be made by coherency or covariance matrix [63][64]

4.3.3.2. Decomposition of Scattering Matrix

Decomposition of scattering matrix into coherency matrix depends on the target properties as the target should be incoherent. In the vigorously varying environment, many target are dependent on their temporal and spatial variations. For those targets, second order moments can be extracted through coherency matrix (T). The coherency matrix can be produced from scattering matrix (S) in of vector form with the help of Pauli's target vector (k). Coherency matrix which is a second order moment is generated by product of first order feature vector (target vector) with its complex conjugate transpose (k^\dagger) as in equation (4.24)

$$k = \frac{1}{\sqrt{2}} \begin{bmatrix} S_{HH} + S_{VV} \\ S_{HH} - S_{VV} \\ 2S_{HV} \end{bmatrix} \quad (4.24)$$

Pauli's target vector is multiplied with its complex conjugate as in equation (4.25)

$$T = k \times k^\dagger \quad (4.25)$$

So the coherency matrix (T) can be estimated by assuming reciprocity condition as in equation (4.26)

$$[T] = \frac{1}{2} \begin{bmatrix} \langle |S_{HH} + S_{VV}|^2 \rangle & \langle (S_{HH} + S_{VV})(S_{HH} - S_{VV})^* \rangle & \langle 2(S_{HH} + S_{VV})S_{HV}^* \rangle \\ \langle (S_{HH} - S_{VV})(S_{HH} + S_{VV})^* \rangle & \langle |S_{HH} - S_{VV}|^2 \rangle & \langle 2(S_{HH} - S_{VV})S_{HV}^* \rangle \\ \langle 2S_{HV}(S_{HH} + S_{VV})^* \rangle & \langle 2S_{HV}(S_{HH} - S_{VV})^* \rangle & \langle 4|S_{HV}|^2 \rangle \end{bmatrix} \quad (4.26)$$

Where, † refers to complex conjugate transpose, <> refers to ensemble averaging, * refers to complex conjugate. The total power also known as span can be represented by the sum of all diagonal elements.

4.3.3.3. Decomposition Modelling

Decomposition modelling of fully PolSAR data using coherency matrix helps to extract the scattering mechanisms. These scattering mechanisms are surface, double bounce and volume scattering which can be obtained by Freeman-Durden decomposition algorithm [10]. A modified version of Freeman-Durden decomposition is given by Yamaguchi *et al.* in which helix scattering also accounted [65]. Yamaguchi decomposition algorithm which gives four type of scattering named as volume, double bounce, surface and helix scattering known as four component decomposition model [65]. This four component decomposition modelling does not obey condition of reflection symmetry.

This decomposition modelling follow the basis coherency matrices obtained from component of surface, double bounce, volume and helix scattering. The expansion of this modelling involves the total power as the weighted sum of individual power obtained from their respective scattering as in equation (4.27) [22].

$$\langle [T] \rangle = f_s \langle [T] \rangle_{surface} + f_d \langle [T] \rangle_{double} + f_v \langle [T] \rangle_{volume} + f_c \langle [T] \rangle_{helix} \quad (4.27)$$

Where, <[T]> represents the coherency matrix, <[T]>_{surface} represents surface scattering <[T]>_{double}, represents the double bounce scattering, <[T]>_{volume} represents volume scattering and <[T]>_{helix} represents the helix scattering. While f_s , f_d , f_v and f_c are the expansion coefficient of surface, double bounce, volume and helix scattering respectively [65].

The basis coherency matrix for surface scattering due to moderately rough surface under Bragg's scattering given in Yamaguchi et al., in [65] as in equation (4.28)

$$\langle [T] \rangle_{surface} = \frac{1}{4} \begin{bmatrix} 1 & \beta^* & 0 \\ \beta & |\beta|^2 & 0 \\ 0 & 0 & 0 \end{bmatrix} \quad (4.28)$$

Where $\beta = \frac{R_H - R_V}{R_H + R_V}$ and R_H and R_V are known as Fresnel reflection coefficient with horizontal and vertical polarization respectively [22].

The basis coherency matrix of double bounce scattering due to dihedral corner reflector is given in equation (4.29)(Yamaguchi, 2006);

$$\langle [T] \rangle_{double} = \frac{1}{4} \begin{bmatrix} |\alpha|^2 & \alpha & 0 \\ \alpha^* & 1 & 0 \\ 0 & 0 & 0 \end{bmatrix} \quad (4.29)$$

Where $\alpha = \frac{S_{HH}+S_{VV}}{S_{HH}-S_{VV}}$ and $|\alpha| < 1$

The basis coherency matrix of volume scattering due to randomly oriented dipoles given as in equation (4.30) [66];

$$\langle [T] \rangle_{volume} = \frac{1}{4} \begin{bmatrix} 2 & 0 & 0 \\ 0 & 1 & 0 \\ 0 & 0 & 0 \end{bmatrix} \quad (4.30)$$

The helix scattering which is not included in three component decomposition was added in four component decomposition model [65] which was implemented from Krogager decomposition algorithm follow the condition of reflection symmetry [66] [65] as;

$$\langle S_{HH}S_{HV}^* \rangle = \langle S_{VV}S_{HV}^* \rangle = 0$$

The basis coherency matrix of helix scattering is given as in equation (4.31) [65];

$$\langle [T] \rangle_{helix} = \frac{1}{2} \begin{bmatrix} 0 & 0 & 0 \\ 0 & 1 & -j \\ 0 & \pm j & 1 \end{bmatrix} \quad (4.31)$$

By using basis coherency matrices of their respective scattering, equation (4.24) can be represented as;

$$\langle [T] \rangle = \frac{f_s}{4} \begin{bmatrix} 1 & \beta^* & 0 \\ \beta & |\beta|^2 & 0 \\ 0 & 0 & 0 \end{bmatrix} + \frac{f_d}{4} \begin{bmatrix} |\alpha|^2 & \alpha & 0 \\ \alpha^* & 1 & 0 \\ 0 & 0 & 0 \end{bmatrix} + \frac{f_v}{4} \begin{bmatrix} 2 & 0 & 0 \\ 0 & 1 & 0 \\ 0 & 0 & 0 \end{bmatrix} + \frac{f_c}{2} \begin{bmatrix} 0 & 0 & 0 \\ 0 & 1 & -j \\ 0 & \pm j & 1 \end{bmatrix} \quad (4.32)$$

The expansion coefficient f_s , f_d , f_v and f_c can be determined as [65];

Expansion coefficient of volume scattering (f_v) can be represented as in equation (4.33);

$$f_v = 8\langle |S_{HV}|^2 \rangle - 4|Im\langle (S_{HH} - S_{VV})S_{HV}^* \rangle| \quad (4.33)$$

Expansion coefficient of double bounce scattering (f_d) represented as;

$$f_d = \frac{1}{2} \langle |S_{HH} - S_{VV}|^2 \rangle - 2 \langle |S_{HV}|^2 \rangle \quad (4.34)$$

Expansion coefficient of helix scattering f_c can be given as;

$$f_c = 2 |Im((S_{HH} - S_{VV})S_{HV}^*)| \quad (4.35)$$

Expansion coefficient of surface scattering (f_s) which is dependent on double bounce scattering can be expressed as (Yamaguchi et al., 2006)

$$f_s = \frac{1}{2} \langle |S_{HH} + S_{VV}|^2 \rangle - 4 \langle |S_{HV}|^2 \rangle - \frac{\left| \frac{1}{2} \langle (S_{HH} + S_{VV})(S_{HH} - S_{VV})^* \rangle \right|^2}{f_d} \quad (4.36)$$

The scattering power associated with the surface, double bounce, volume and helix scattering are P_s , P_d , P_v and P_c respectively. The scattering power can be represented in terms of their respective expansion coefficient as [22];

$$P_s = f_s(1 + |\beta|^2) \quad (4.37)$$

$$P_d = f_d(1 + |\alpha|^2) \quad (4.38)$$

$$P_v = f_v \quad (4.39)$$

$$P_c = f_c \quad (4.40)$$

The total scattering power is the sum of power of all scattering. The total scattering power (P_t) can be represented as;

$$P_t = P_s + P_v + P_d + P_c \quad (4.41)$$

This total scattering power is the power generated from all the scattering like surface, volume, double bounce and helix scattering.

4.3.4. Modelling Approach for AGB estimation

This section is grouped in two subsections. The first subsection is a detailed description of modelling approach by applying Water Cloud Model and admitting canopy gaps in Water Cloud Model. The second subsection is a detailed description of Extended Water Cloud Model by implying higher order scattering mechanisms as stem to ground interactions or ground to stem interactions. The section also provide the information for implication of Hybrid PolSAR data and fully PolSAR data in modelling approach of Water Cloud Model for retrieving forest biophysical parameters.

4.3.4.1. Water Cloud Model (WCM)

The Water Cloud Model conception was first formulated by Attemma and Ulaby [47]. The concept of this model describes the relationship between forest biophysical parameters and the retrieved backscatter from vegetation. The basic premise of WCM is that the vegetation acts as a homogenous medium occupied by droplets of water. These droplets are assumed to be uniformly dispersed over horizontal plane surface that signifies ground surface. The incoming energy of EM wave incident upon the upper layer of the medium is partly transmitted back to the sensor and partly to the lower layer. Portion of the energy which is transmitted to lower layer is the attenuation of vegetation block. The model considers that all scatters follow the similar properties. This infers that the attenuation cross section and total cross section of radar endure same for all scatters. This implies that the total backscattered energy is characterised by the incoherent amount of scattered energy at each layer. Following are the key properties of WCM given by Santoro *et al.*, [67]:

- WCM does not comprise multiple reflections. Even bounce scattering between ground and vegetation i.e. higher order scattering are not included.
- It considers only surface scattering from ground and from vegetation i.e. single scattering.
- WCM considers vegetation as a homogenous medium. The gaps between canopies are excluded.
- The water droplets in cloud are constituted by similar particles and thus consider as a homogenous medium.

The WCM simply expressed as (Leeuwen, 1991):

$$\sigma_{for}^0 = \sigma_{veg}^0 + \sigma_{gr}^0 T_{tree} \quad (4.42)$$

Where, σ_{for}^0 = The forest backscatter

σ_{veg}^0 = The backscatter from vegetation

σ_{gr}^0 = Backscatter from ground and

T_{tree} = The two way transmissivity of tree.

Based on radiative transfer theory, another model was developed including canopy gaps which is similar to WCM. Water cloud model can be expressed including canopy gaps as [68];

$$\sigma_{for}^0 = (1 - \eta)\sigma_{gr}^0 + \eta[\sigma_{gr}^0 T_{tree} + \sigma_{veg}^0 (1 - T_{tree})] \quad (4.43)$$

Where, η = Area fill factor.

On the basis of scattering from ground and scattering from vegetation, the water cloud model is shown in Figure 4-4. The incoming wave incident upon the top canopy layer and interacts with the canopy layer and then transmitted back by canopy surface to the sensor is expressed by σ_{veg}^0 . The incoming wave incident

upon the ground surface and transmitted back to the sensor is represented as σ_{gr}^0 i.e. backscattering from ground surface.

Using area fill factor and the two way transmissivity, the WCM can be expressed as [3] [69];

$$\sigma_{for}^0 = \sigma_{gr}^0 e^{-\beta B_{AGB}} + \sigma_{veg}^0 (1 - e^{-\beta B_{AGB}}) \quad (4.44)$$

Where, β = empirically defined coefficient.

B_{AGB} = aboveground biomass.

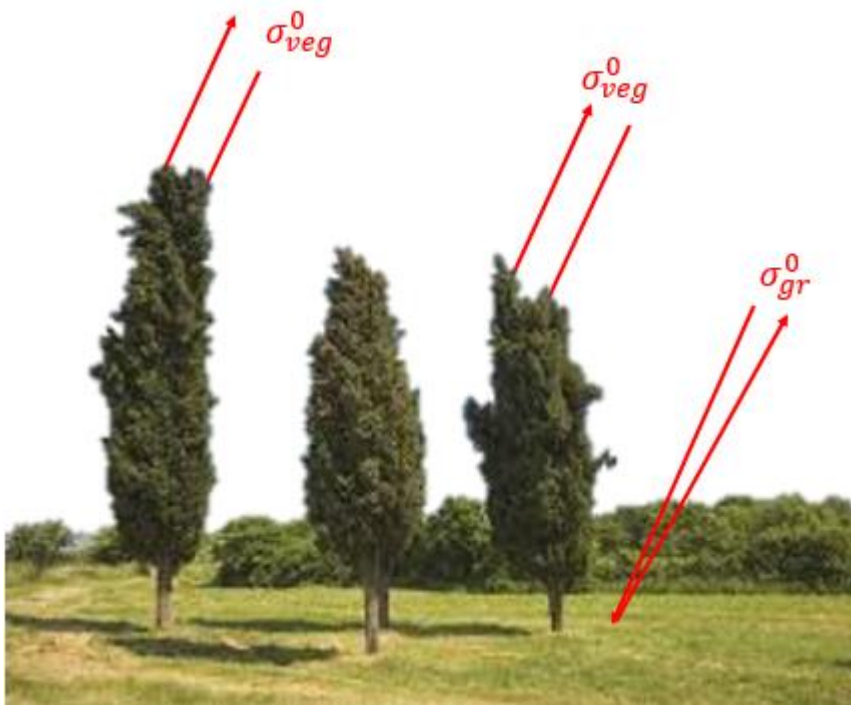


Figure 4-4: Backscatter from upper canopy (σ_{veg}^0) and from ground (σ_{gr}^0) in WCM

The two way attenuation for forest can be represented as inverse exponential of product of aboveground biomass " B_{AGB} " and empirically defined coefficient " β " [3] [69].

4.3.4.2. Extended Water Cloud Model (EWCM)

Water cloud modelling approach mainly consider backscattering from ground surface and vegetation canopy. WCM doesn't deliberate the higher order scattering like even bounce scattering. Even bounce or double bounce scattering mainly include stem to ground or ground to stem interactions. This should be interpreted by considering a longer wavelength (like L-band) [70]. The present water cloud modelling further extended including canopy gaps for higher order interactions for the vegetation cover.

a) Backscattering retrieval from ground stem interaction from canopy

The backscattering from ground stem interaction involves the interaction of wave with ground first and then wave is reflected towards stem where wave hits the stem and then return back to the sensor. Another interaction may also occur in which incident wave hit the stem first and then reflected towards the ground where again it get reflected back towards the sensor. In both the cases this higher order interaction is named as double bounce scattering or even bounce scattering. Figure 4-5 shows that the incoming incident wave interacts with ground surface and reflected towards stem where it hits the stem and again reflected towards the sensor.

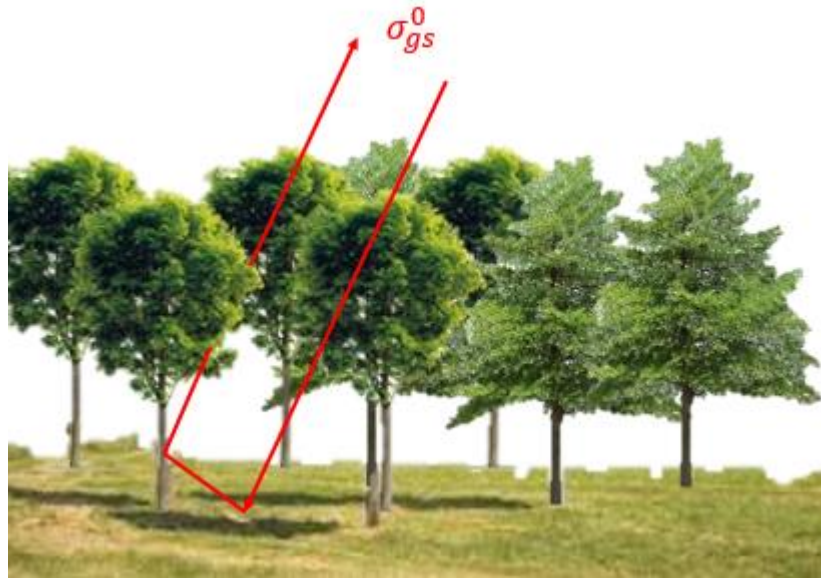


Figure 4-5: Backscattering from ground stem interaction (σ_{gs}^0) through canopy

This backscattering contribution of such ground stem interactions can be expressed as

$$\eta \sigma_{gs}^0 T_{tree} \tag{4.45}$$

Where, η = The fraction of ground which is covered by canopy layer.

σ_{gs}^0 = Backscattering from ground stem interactions.

T_{tree} = Two way transmissivity of tree.

b) Backscattering retrieval from ground stem interactions from canopy gaps

This backscattering involves the interaction of wave with ground and reflected towards the stem where it hits the stem and reflected back to the sensor through the gaps in the canopy. Figure 4-6 shows that the wave incident upon ground surface and reflected towards the stem where it hits and again reflected back towards the sensor through the canopy gaps.

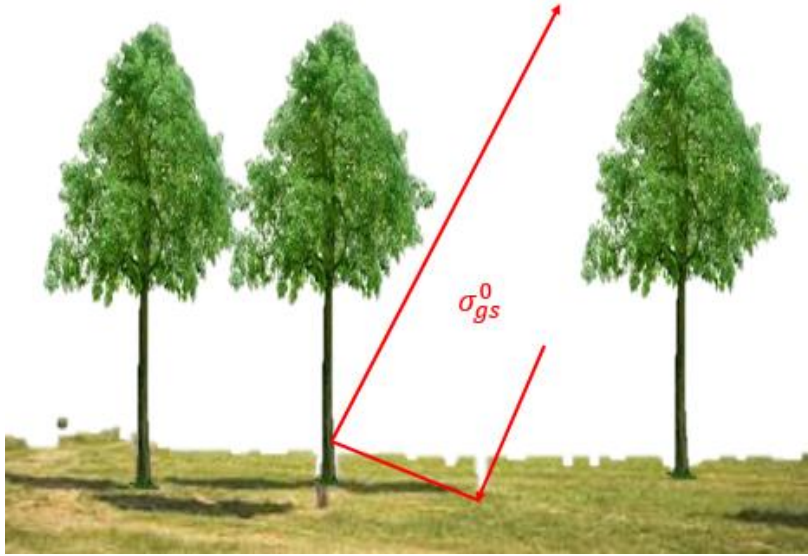


Figure 4-6: Ground stem interaction through (σ_{gs}^0) canopy gaps

The backscattering contribution through the canopy gaps can be expressed as

$$(1 - \eta)\sigma_{gs}^0 \quad (4.46)$$

Where, $(1 - \eta)$ refers to the fraction of ground surface which is not covered by the canopy and σ_{gs}^0 refers to the ground stem backscattering.

The extended water cloud modelling can be expressed including higher order interaction as [22];

$$\sigma_{for}^0 = \sigma_{gr}^0 e^{-\beta B_{AGB}} + \sigma_{veg}^0 (1 - e^{-\beta B_{AGB}}) + \sigma_{gs}^0 e^{-\beta B_{AGB}} \quad (4.47)$$

Where, β = empirically defined coefficient.

B_{AGB} = aboveground biomass.

To retrieve the scattering information, PolSAR images are decomposed so that the constituent scattering can be extracted from those images. The scattering mechanisms involved in the decomposition techniques used in this study consist of surface scattering, volume scattering and double bounce scattering. The EWCM model fits because it involves the contribution of double bounce scattering also which can't be included in WCM. There are four unknown parameters in equations (4.47) as;

- Backscattering from vegetation (σ_{veg}^0)

- Backscattering from ground stem interactions (σ_{gs}^0)
- Backscattering from ground surface (σ_{gr}^0)
- Empirically defined coefficient (β)

To simplify the model, unknown parameters are reduced using components which obtained from polarimetric decomposition. Vegetation backscattering which is generated from upper canopy is modelled using volume scattering obtained from decomposition. Backscattering from ground stem interactions which basically generated from interaction of wave with ground and then with stem is modelled using double bounce scattering from decomposition. The backscattering from ground surface which occur due to interaction of wave with bare ground or from the ground visible from the canopy gaps is modelled using surface scattering component from decomposition [22]. Total forest backscatter is the backscattering from forest which indicate total power and can be obtained by summing all decomposition components.

Above mentioned process help in reducing the unknown parameters to one. The only remaining unknown parameter is empirically defined coefficient “ β ”. This coefficient will be estimated distinctly for modelling of AGB.

5. RESULTS

This Chapter gives a brief description of the results obtained from this study. The results consists of field data and decomposition components obtained from the Hybrid PolSAR data and fully PolSAR data. This chapter also describes semi empirically defined coefficient (β) and biophysical parameter (AGB) retrieval using semi empirical modelling (WCM) with the accuracy assessment of Hybrid PolSAR results from field data as well as from fully PolSAR data.

5.1. Hybrid Polarimetric Decomposition Components and Results

This section gives a detailed description of the results obtained from Hybrid polarimetric decomposition techniques in aspects of their decomposition components.

5.1.1. m-delta (m- δ) decomposition

The m-delta decomposed images of different scatterings obtained from the Barkot forest area are shown in Figure 5-1 (a), Figure 5-1 (b) and Figure 5-2 (a). The shown images are grey values mages.

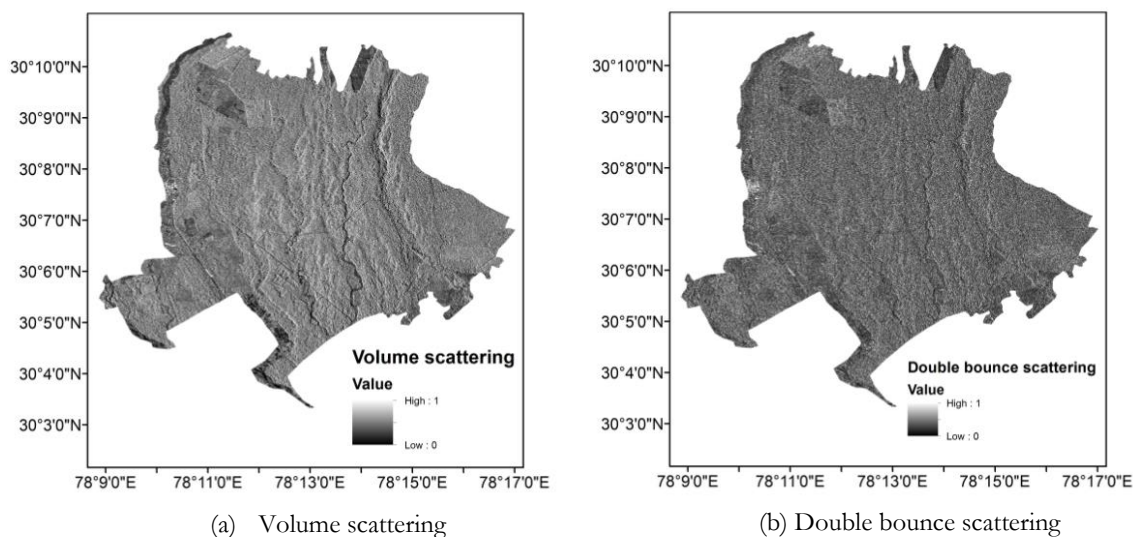


Figure 5-1: (a) Volume scattering image from m-delta decomposition (b) Double bounce scattering from m-delta decomposition

Figure 5-1 (a) is the representation of the volume scattering occur from the upper canopy cover. The scattering which occur due to ground to stem or stem to ground interactions is shown in Figure 5-1 (b). Scattering results as a decomposed component from the ground surface is shown in Figure 5-2 (a).

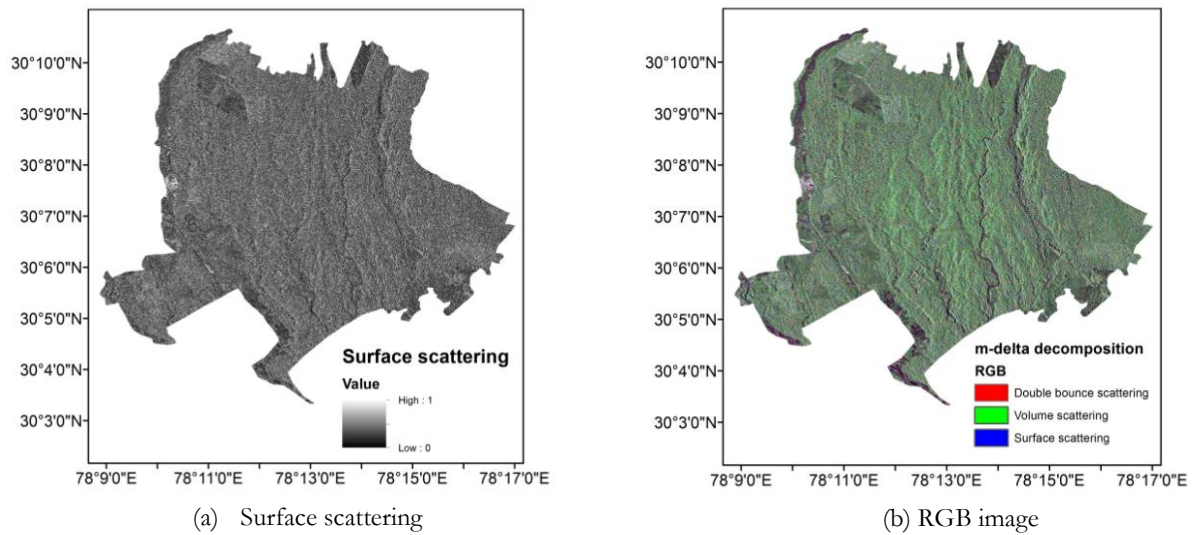


Figure 5-2: (a) Surface scattering image obtained from m-delta decomposition (b) RGB colour coded image of m-delta decomposition

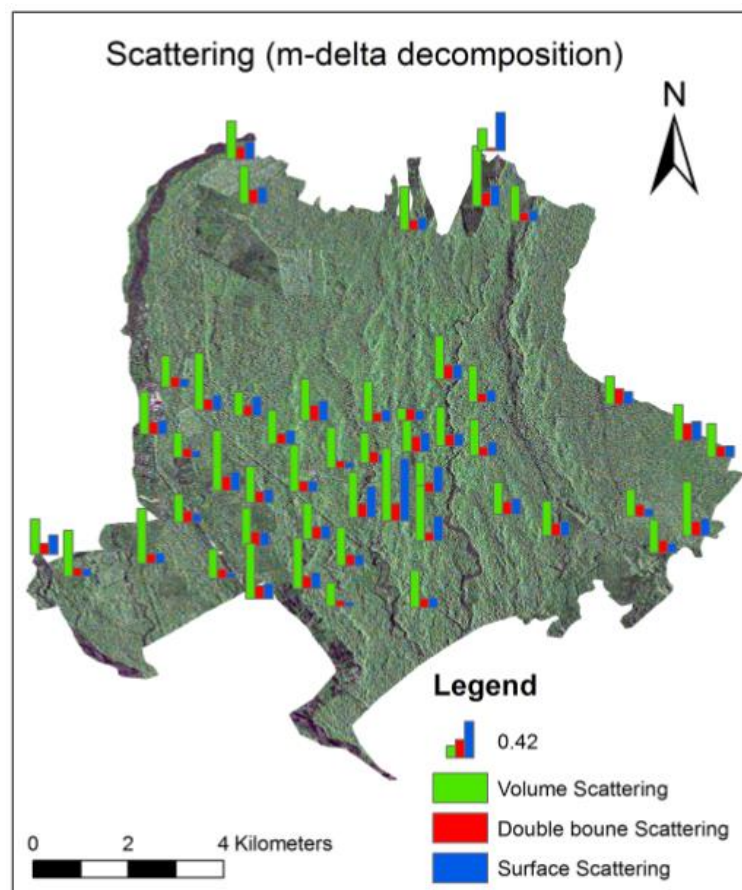


Figure 5-3: Contribution of surface, double bounce and odd bounce scattering for each sample plot.

Figure 5-2 (b) is showing the RGB colour coded image based on the Backscattering Aspect (BSA) convention is obtained after applying the m-delta decomposition in which red pixel is an indication of

double bounce scattering, green is an indication of volume scattering and blue is an indication of odd bounce or surface scattering. Figure 5-3 is showing the backscatter value of surface, double bounce and volume scattering from each sample plots collected in the Barkot forest area implying high value of backscatter for volume scattering.

5.1.2. m-chi (m- χ) decomposition

The m-chi decomposed image obtained from volume scattering, double bounce scattering and surface scattering for the Barkot forest are shown in Figure 5-4 (a), Figure 5-4 (b) and Figure 5-5 (a) respectively.

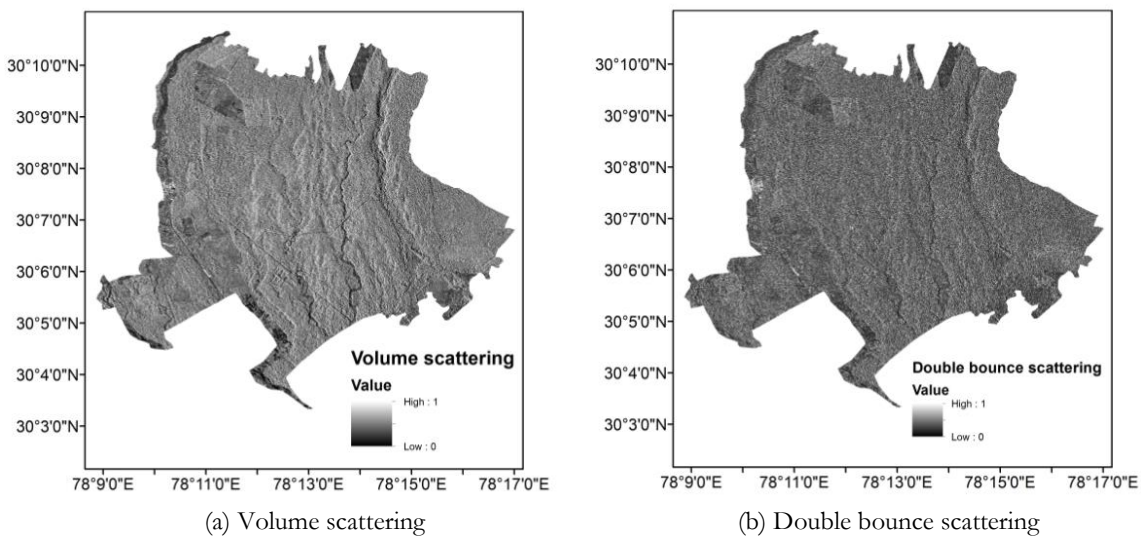


Figure 5-4: (a) Volume scattering image obtained from m-chi decomposition (b) Double bounce scattering image obtained from m-chi decomposition

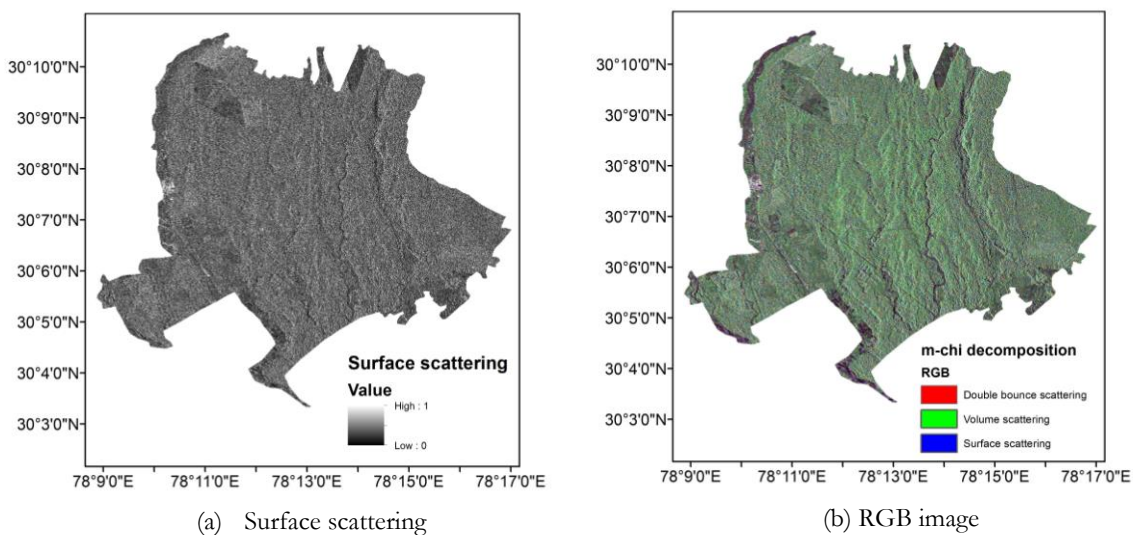


Figure 5-5: (a) Surface scattering image obtained from m-chi decomposition (b) RGB image obtained from m-chi decomposition

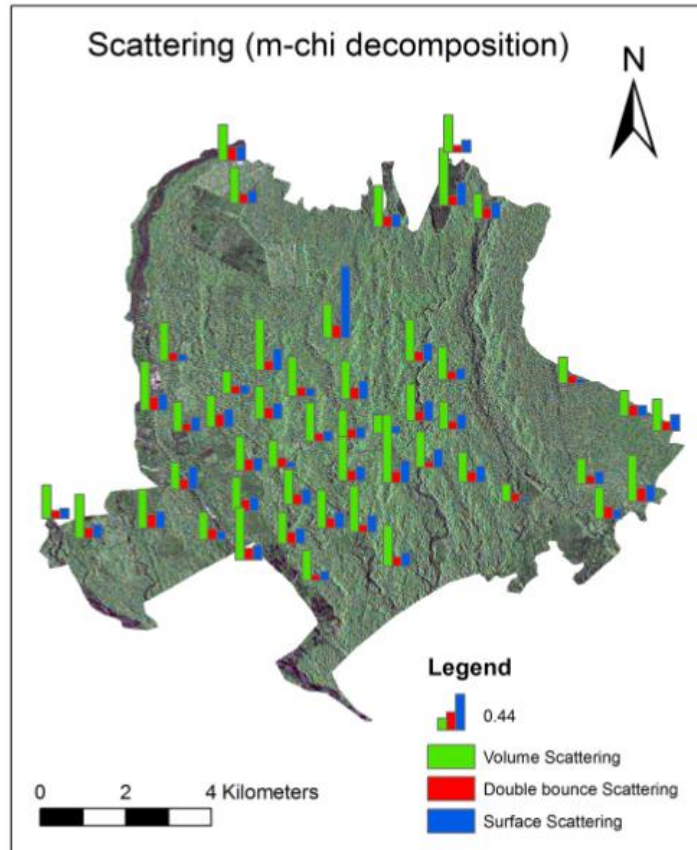


Figure 5-6: Volume, surface and double bounce scattering obtained after m-chi decomposition from all the sample plots

All the scattering images shown in Figure 5-4 (a), Figure 5-4 (b) and Figure 5-5 (a) are grey level images. The RGB colour coded image obtained after m-chi decomposition is shown in Figure 5-5 (b). RGB colour coded image provide the scattering information as red colour of pixel is showing the contribution of double bounce scattering, green colour of pixel is an indication of volume scattering contribution and blue colour of pixel is showing the contribution of surface scattering. The contribution of the surface, volume and double bounce scattering from all the collected sample plots is shown in Figure 5-6. The Figure 5-6 is showing the contribution of all scattering for each plot which means all the shown backscatter value are based on the location chosen for each sample plot.

5.1.3. m-alpha ($m-\alpha$) decomposition

The m-alpha decomposed images of volume scattering, double bounce scattering and surface scattering is shown in Figure 5-7 (a), Figure 5-7 (b) and Figure 5-8 (a) respectively. The mentioned images are showing the contribution as per their scattering target. Images shown in Figure 5-7 (a), Figure 5-7 (b) and Figure 5-8 (a) are the grey level images.

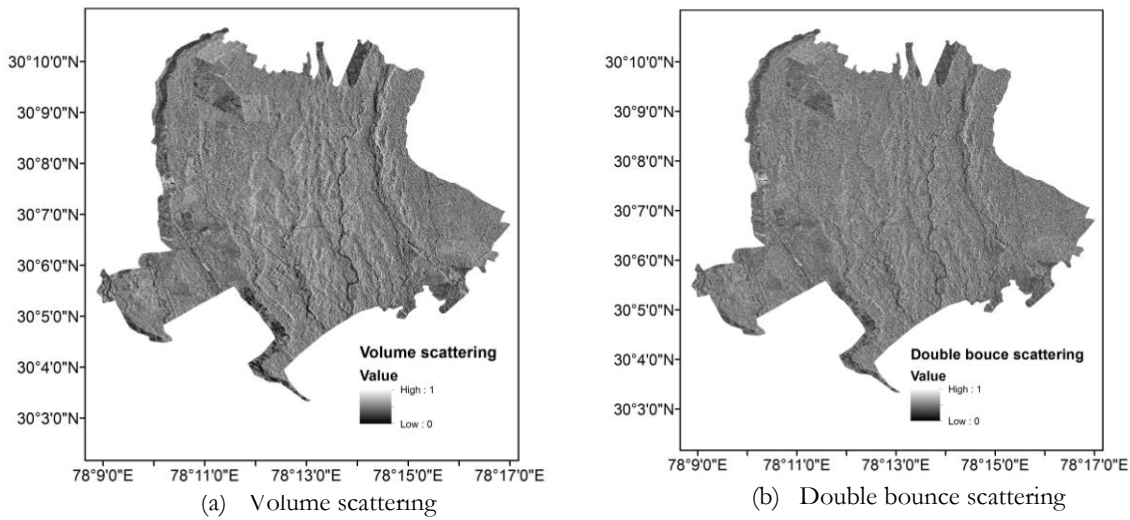


Figure 5-7: (a) Volume scattering image obtained from m-alpha decomposition (b) Double bounce scattering image from m-alpha decomposition

The RGB colour coded image obtained after m-alpha decomposition of Hybrid PolSAR data is shown in Figure 5-8 (b). The red colour of pixel in RGB image is showing the contribution of double bounce scattering, green colour of pixels is representing volume scattering at that location and blue colour of pixels is an indication of surface scattering from that location. Figure 5-9 is the representation of all the scattering retrieved from the sample plots collected in Barkot forest area in which volume scattering is dominant.

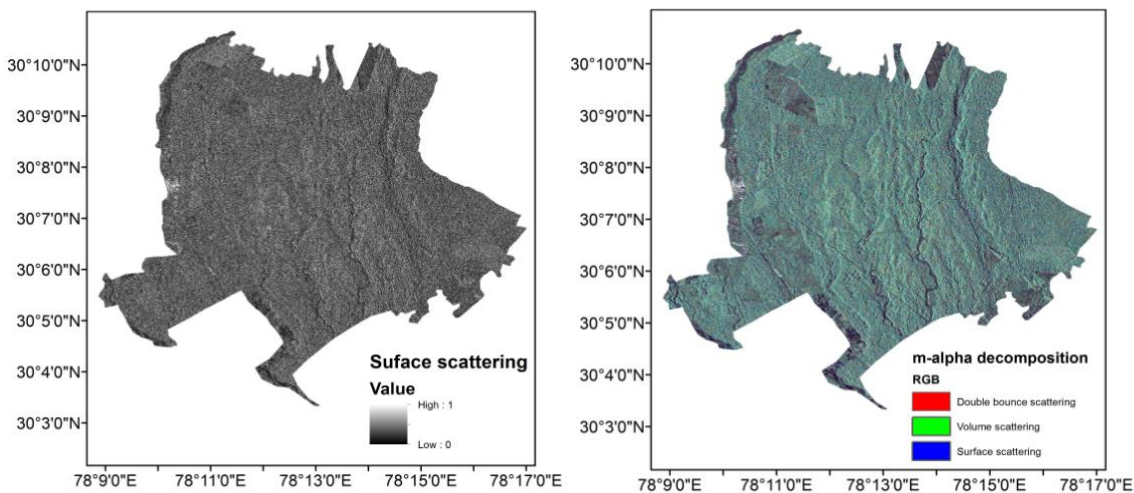


Figure 5-8: (a) Surface scattering image obtained from m-alpha decomposition (b) RGB colour coded image obtained from m-alpha decomposition

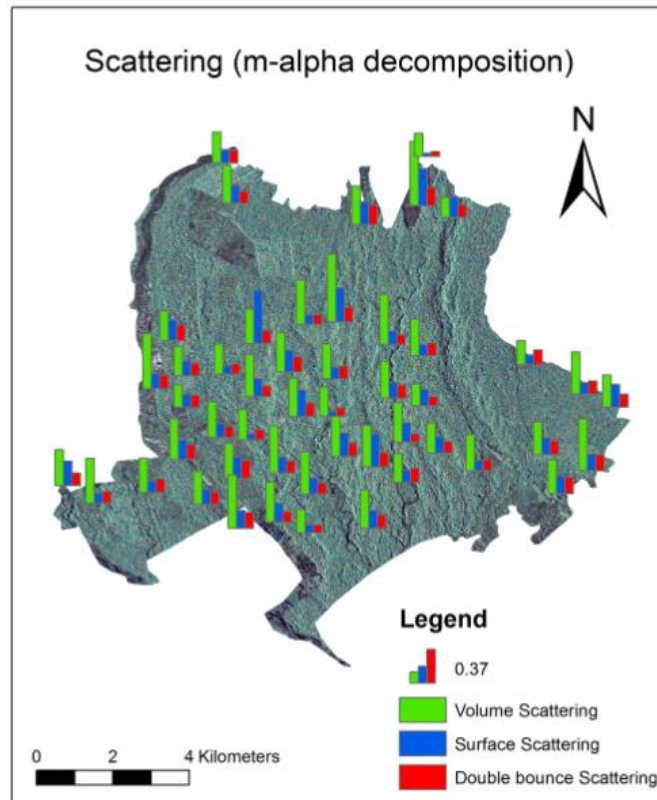


Figure 5-9: Scattering information retrieved from m-alpha decomposition

5.2. Fully Polarimetric Decomposition Components and Results

Decomposition components obtained after Yamaguchi four component decomposition modelling of fully polarimetric data of Radarsat-2 are volume scattering, double bounce scattering, double bounce scattering and helix scattering shown in Figure 5-10 (a), Figure 5-10 (b) and Figure 5-11 (a) respectively.

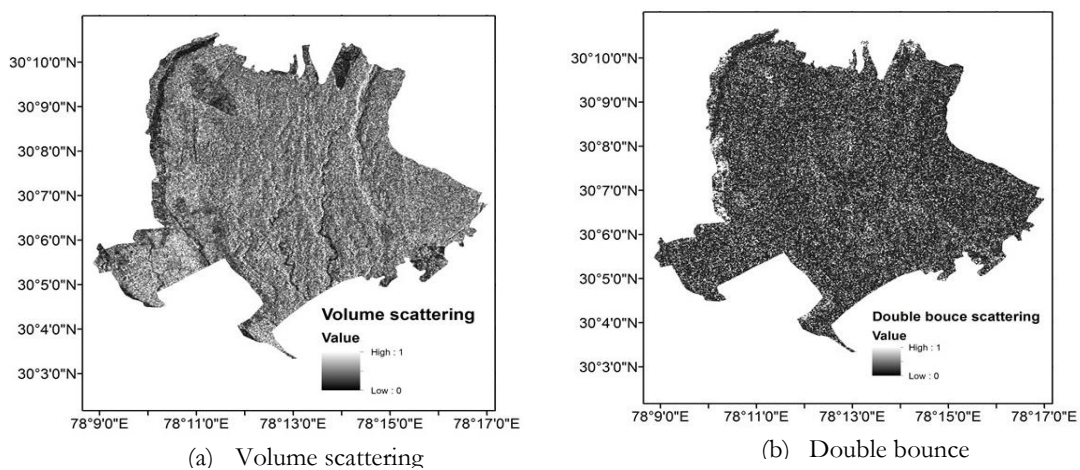


Figure 5-10: (a) Volume scattering image obtained from Yamaguchi decomposition (b) Double bounce scattering image obtained from Yamaguchi decomposition of Radarsat-2 data.

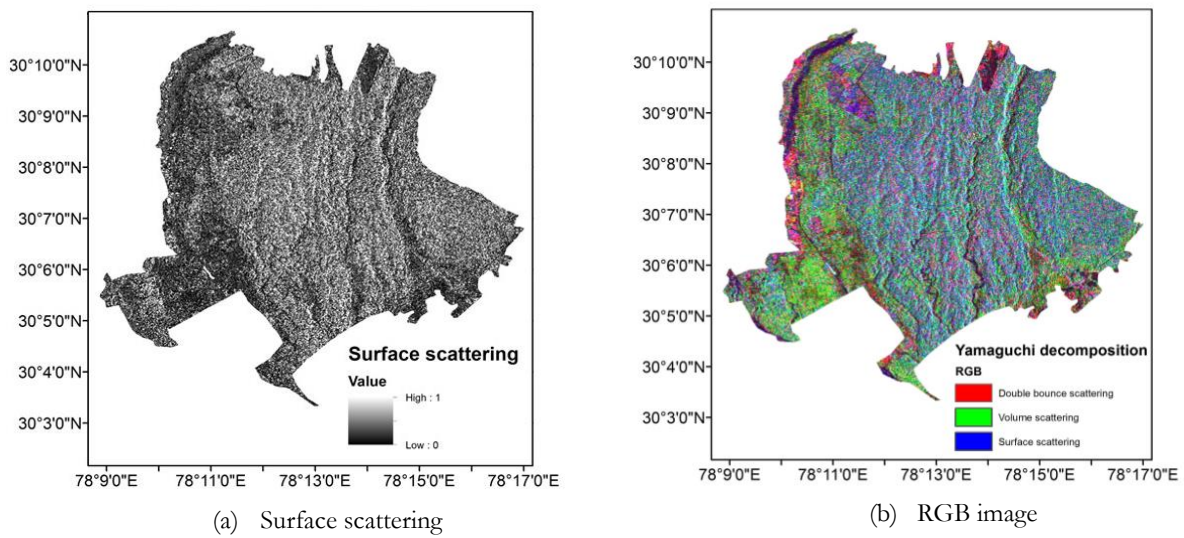


Figure 5-11: (a) Surface scattering image obtained from Yamaguchi decomposition of fully polarimetric data (b) RGB colour coded image obtained from Yamaguchi decomposition of fully polarimetric data.

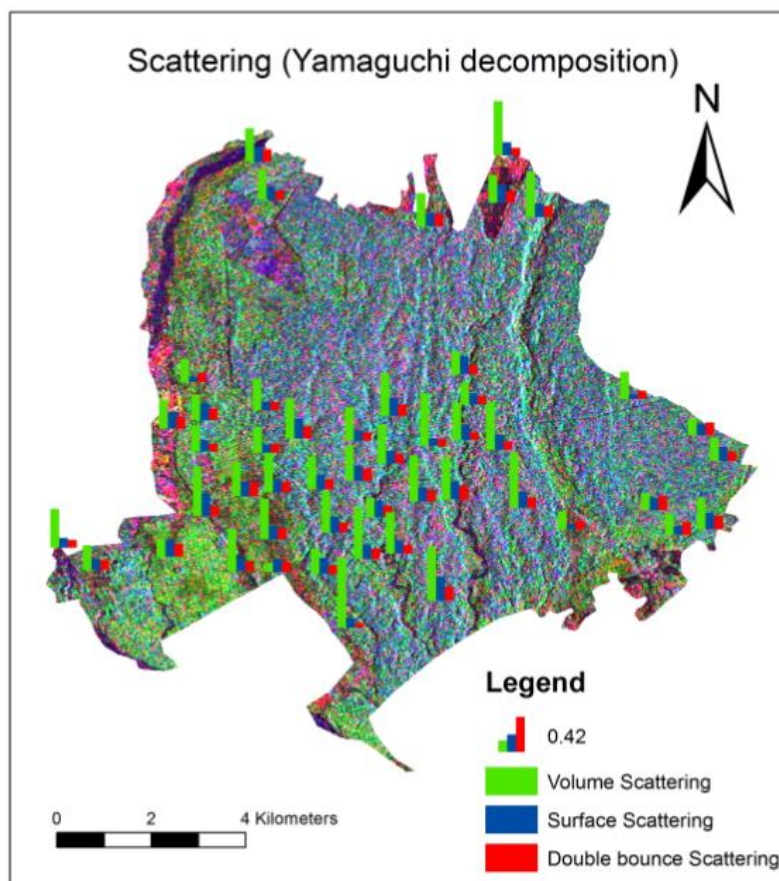


Figure 5-12: Scattering retrieved from the Yamaguchi decomposition for fully polarimetric data.

The RGB colour coded image of Yamaguchi decomposition modelling is shown in Figure 5-11 (b). Figure 5-11 (b) depicts that the red colour of pixel is double bounce scattering, blue colour of pixel is showing

surface scattering and green colour of pixel is volume scattering. Figure 5-12 represents the scattering contribution from all scatterers for each sample plot in the Barkot forest area.

5.3. Comparisons of Decomposition Components

The results obtained from the decomposition modelling in aspect of scattering retrieved from each decomposition is given in Figure 5-13, Figure 5-14 and Figure 5-15.

5.3.1. Volume Scattering:

Figure 5-13 represents the variations in backscatter value among volume scattering retrieved from the m-delta, m-chi, m-alpha and Yamaguchi decomposition. The maximum and minimum backscatter value obtained from m-delta decomposition are 0.833 and 0.141 respectively with the mean value as 0.447. The m-chi decomposition is also showing maximum backscatter value as 0.833 with minimum backscatter value as 0.218. The mean backscatter value obtained from m-chi is 0.433. Backscatter value obtained from m-alpha is 0.732, 0.219 and 0.403 as maximum, minimum and mean backscatter value respectively. Volume scattering obtained from Yamaguchi decomposition represents maximum and minimum backscatter value as 0.846 and 0.103 respectively with the mean backscatter value as 0.416.

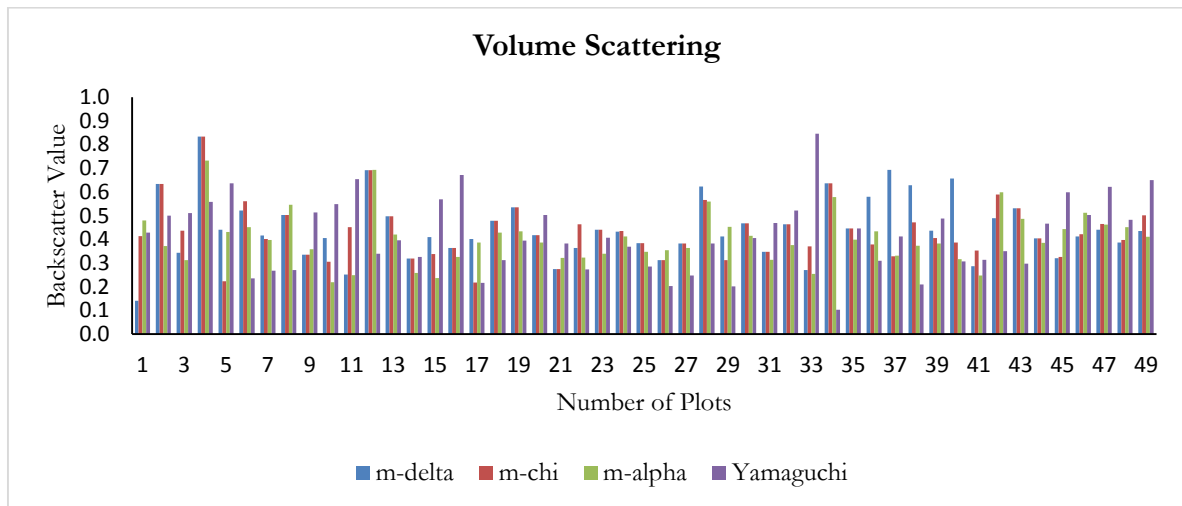


Figure 5-13: Comparison of volume scattering with all decomposition methods used in this study

5.3.2. Double Bounce Scattering:

Figure 5-14 is the representation of variations in backscatter value among double bounce scatterings retrieved from all decomposition methods used in this study. The double bounce scattering retrieved from m-delta decomposition is showing maximum and minimum backscatter value as 0.2 and 0.032 with mean backscatter value as 0.131. The m-chi decomposition is providing maximum and minimum backscatter value as 0.17 and 0.07 respectively with the mean value as 0.119. The backscattering retrieved from m-alpha decomposition is showing 0.215 as maximum and 0.051 as minimum value with the 0.138 as mean

backscatter value. Yamaguchi is showing 0.173 as maximum, 0.06 as minimum and 0.126 as mean backscatter value.

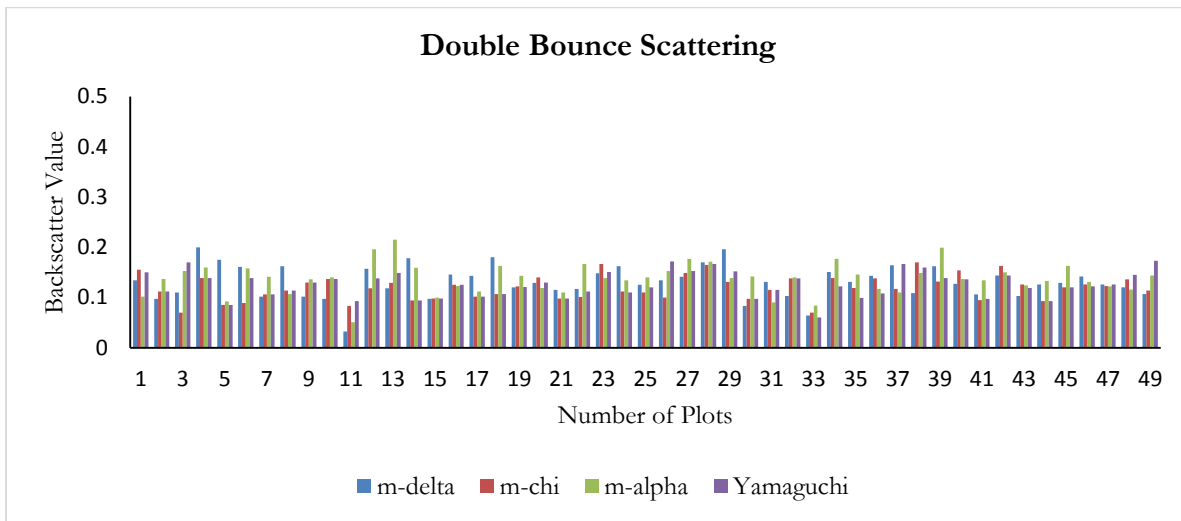


Figure 5-14: Comparison in double bounce scattering with all decomposition methods used in this study

5.3.3. Surface Scattering:

The surface scattering retrieved from all decompositions are shown in Figure 5-15.

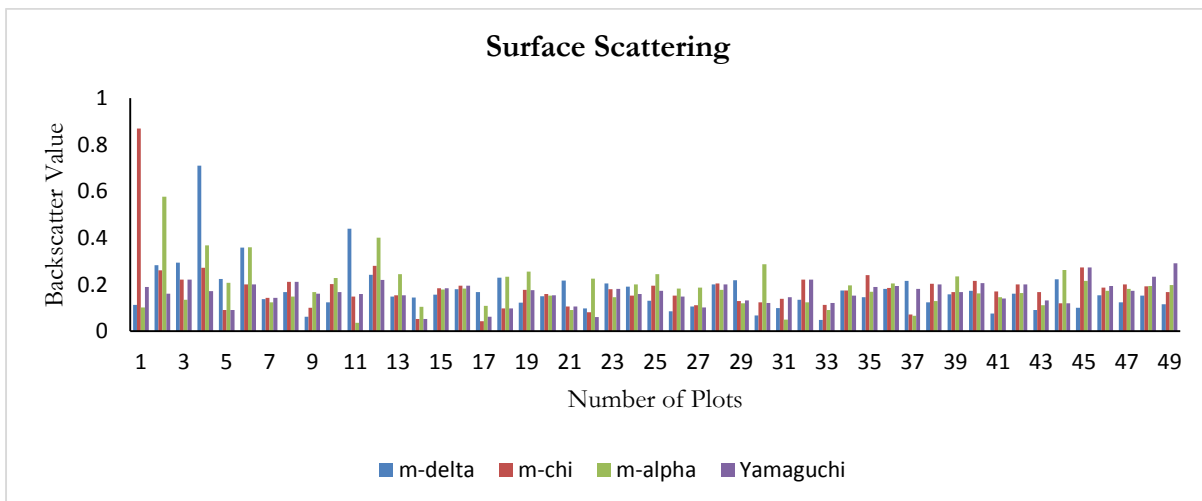


Figure 5-15: Comparison of surface scattering among all decompositions used in this study.

Figure 5-15 describes that m-delta decomposition is giving 0.71 as maximum backscatter value, 0.048 as minimum backscatter value and 0.176 as mean of the volume scattering. The retrieved backscatter value from m-alpha ranges from 0.036 to 0.577 with the mean backscatter value 0.188. The m-chi decomposed component ranges from 0.042 to 0.87 as backscatter value for surface scattering with 0.182 as mean

backscatter value. The surface scattering retrieved from Yamaguchi decomposition ranges from 0.052 to 0.291 with 0.165 as mean value.

5.4. Relationship between Volume Scattering and Field Biomass

As the volume scattering has prime contribution to see the vegetation cover in the forest area. Figure 5-16 (a), Figure 5-16 (b) and Figure 5-17 (a) depicts the contribution of volume scattering with the field measured biomass for those sample plots which are taken in the Barkot forest area using Hybrid polarimetric decomposition.

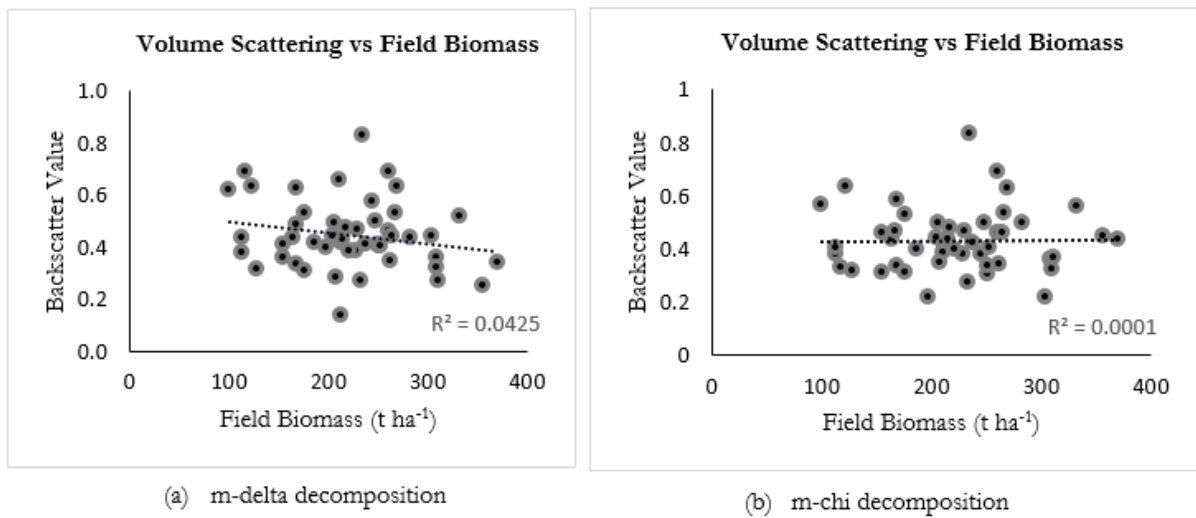


Figure 5-16: (a) Volume scattering obtained using m-delta decomposition against field biomass (b) Volume scattering obtained using m-chi decomposition against field biomass.

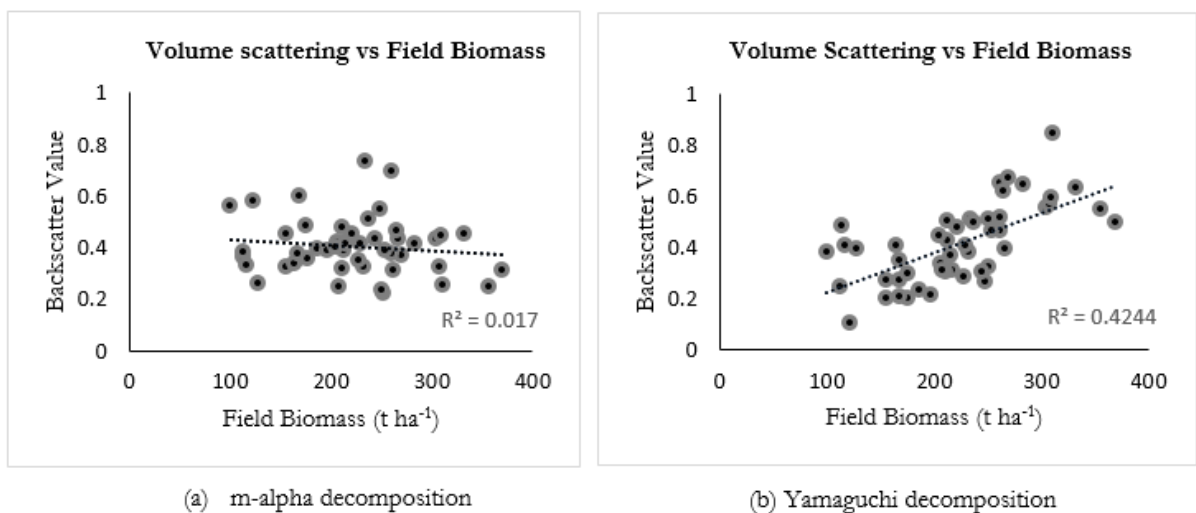


Figure 5-17: (a) Volume scattering obtained using m-alpha decomposition against field biomass (b) Volume scattering obtained using Yamaguchi decomposition against field biomass

The volume scattering retrieved from the m-delta decomposition is showing $R^2 = 0.0425$ with the biomass measured in the field, given in Figure 5-16 (a). After applying m-chi decomposition and retrieving volume scattering is showing $R^2 = 0.0001$ with the field measured biomass depicted in Figure 5-16 (b). Figure 5-17 (a) is showing the $R^2 = 0.017$ between field measured biomass and volume scattering retrieved from m-alpha decomposition. Figure 5-17 (b) depicts the relation between volume scattering retrieved using fully PolSAR data and biomass measured in the field. The volume scattering and field measured biomass is showing $R^2 = 0.4244$.

5.5. Relationship between Total Forest Backscatter and Measured Biomass

The relation of total forest backscatter (σ_{for}^0) calculated from Hybrid PolSAR decomposition methods and fully polarimetric decomposition method with the biomass which was measured in the field is depicted in Figures 5-18 (a), Figure 5-18 (b), Figure 5-19 (a) and Figure 5-19 (b).

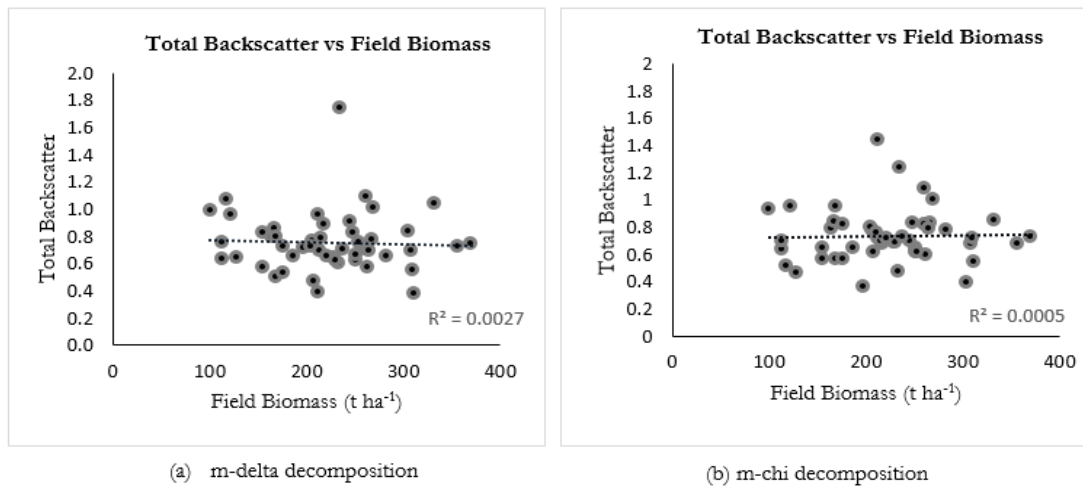


Figure 5-18: (a) Total backscatter obtained from m-delta decomposition against field measured biomass (b) Total backscatter obtained using m-chi decomposition against field measured biomass

The total backscatter obtained from m-delta decomposition given by Figure 5-18 (a) is showing $R^2 = 0.0027$ with the biomass measured in the field. Figure 5-18 (b) and Figure 5-19 (a) is the depiction of the total backscatter retrieved from forest with biomass measured in the field for m-chi and m-alpha decomposition. The m-chi decomposed total backscatter is showing $R^2 = 0.0005$ with field measured biomass. While the R^2 value for total backscatter retrieved from forest with field measured biomass is 0.0036 for m-alpha decomposition. Figure 5-19 (b) is the representation of scatterplot drawn between total backscatter and field measured biomass. The total backscatter retrieved from forest using fully PolSAR data of Radarsat-2 is showing the $R^2 = 0.2839$ with the field measured biomass.

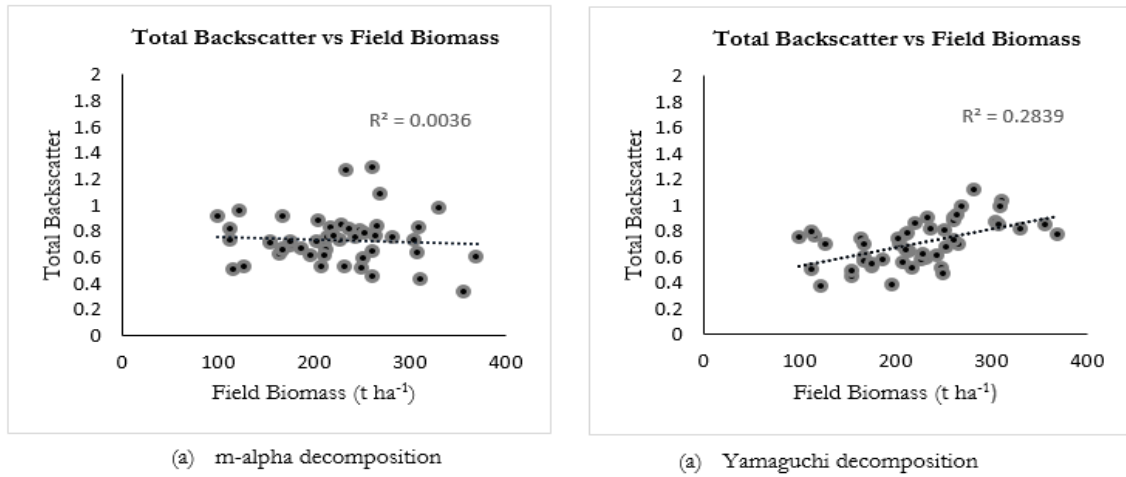


Figure 5-19: Total backscatter using m-alpha decomposition against field measured biomass (b) Total backscatter obtained using Yamaguchi decomposition against field measured biomass

5.6. Parameter estimation of EWCM and Results

There are total five unknown parameters in the extended water cloud model. These are backscattering from canopy cover (σ_{veg}^0), backscattering from ground to stem interactions or stem to ground interactions (σ_{gs}^0), backscattering from ground surface (σ_{gr}^0), total backscattering from forest (σ_{for}^0) empirically defined coefficient (β) and AGB (B_{AGB}). Polarimetric decomposition algorithms used to calculate parameters like σ_{veg}^0 , σ_{gs}^0 , σ_{gr}^0 and σ_{for}^0 which reduces the number of unknown parameters to one i.e. (β). This empirically defined coefficient helps in calculating required AGB.

5.6.1. Retrieval of β

The required backscattering parameters of EWCM are retrieved using the polarimetric decomposition techniques like m-delta, m-chi, m-alpha and Yamaguchi decomposition. The retrieved backscattering is from their respective volume, double bounce and surface targets. The empirically defined coefficient (β) is derived from *in-situ* measurements in the Barkot forest area. There were 49 plots available to perform this study out of which 15 sample plots has been taken into account to calculate the parameter β . Remaining samples plots retained to perform the modelling of AGB.

Those plots which were used to calculate the β parameter are mostly those plots which show less volume scattering with high biomass. To calculate β , same plots are used for each decomposition techniques i.e. m-chi, m-delta, m-alpha and Yamaguchi decomposition. The relation of β parameter with the scattering components, field measured AGB (in-situ measurements) and the total backscatter from forest can be given using equation (4.47) as

$$\beta = -\frac{1}{B_{AGB}} \ln \left(\frac{\sigma_{for}^0 - \sigma_{veg}^0}{\sigma_{gr}^0 - \sigma_{veg}^0 + \sigma_{gs}^0} \right) \quad (5.1)$$

Where, B_{AGB} =Aboveground Biomass (t ha⁻¹).

In this study, for the estimation of β , it was assumed that the double bounce scattering occurs from the vegetation (in the case of forest). As the C-band data was used to perform the study which has low canopy penetration ability than L-band. Hence, the backscatter from ground to stem interactions is added to the backscatter from the vegetation which turned equation (5.1) as;

$$\beta = -\frac{1}{B_{AGB}} \ln \left(\frac{\sigma_{for}^0 - (\sigma_{veg}^0 + \sigma_{gs}^0)}{\sigma_{gr}^0 - \sigma_{veg}^0 + \sigma_{gs}^0} \right) \quad (5.2)$$

The particulars of estimated β values for the all the decompositions such as m-delta, m-chi, m-alpha and Yamaguchi using equation (5.2) is shown in Table (5-1) which will be further used in AGB modelling. The estimated β value for all the remaining sample plots is kept constant as per their polarimetric decomposition. The unit of β parameter is ha/m³.

Table 5-1. Estimated β for AGB modelling

Modelled AGB	β (ha/m ³)			
	m-delta	m-chi	m-alpha	Yamaguchi
	Decomposition	Decomposition	Decomposition	Decomposition
	0.003045	0.003233	0.002853	0.003037

5.6.2. Retrieval of AGB using EWCM

The extended water cloud model is used to model the AGB by upturning the equation (5-1). The β value is used as mentioned in Table (5-1) of their particular decomposition technique for modelling AGB. The EWCM approach is applied on those 39 sample plots which are not included in the β parameter estimation. For modelling AGB including β value, the transformed formula can be given as

$$B_{AGB} = -\frac{1}{\beta} \ln \left(\frac{\sigma_{for}^0 - (\sigma_{veg}^0 + \sigma_{gs}^0)}{\sigma_{gr}^0 - \sigma_{veg}^0 + \sigma_{gs}^0} \right) \quad (5.3)$$

The scatterplots are generated from field measured biomass and modelled AGB. Figure 5-20 (a) depicts the scatterplot of modelled AGB using m-delta decomposition and field biomass. Figure 5-20 (b) represents the scatterplot between modelled AGB using m-chi decomposition and field biomass.

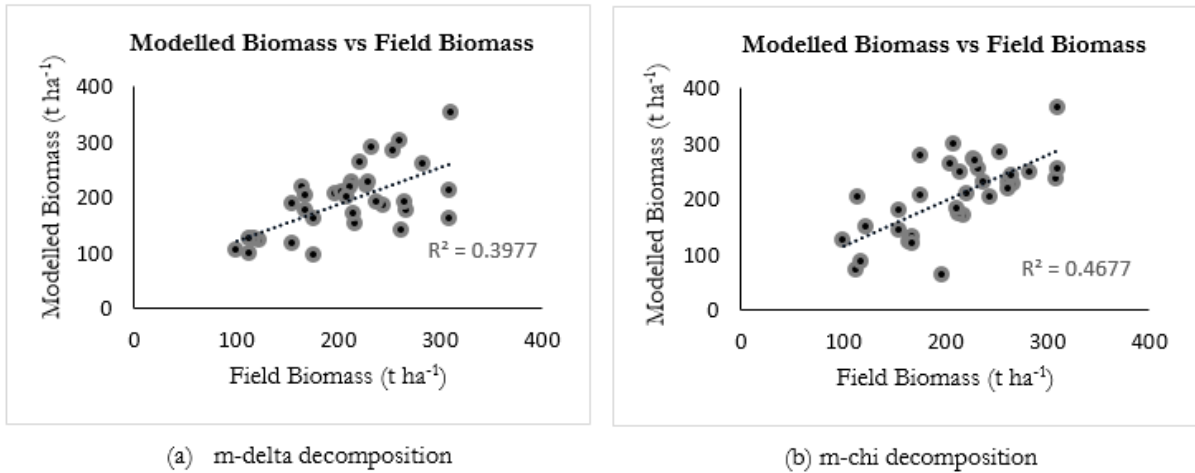


Figure 5-20: (a) Modelled AGB using m-delta decomposition against field biomass (b) Modelled AGB using m-chi decomposition against field biomass

Figure 5-21 (a) shows the scatterplot between modelled AGB using m-alpha decomposition and field measured biomass. Figure 5-21 (b) represents the scatterplot generated between modelled AGB using Yamaguchi decomposition and field biomass.

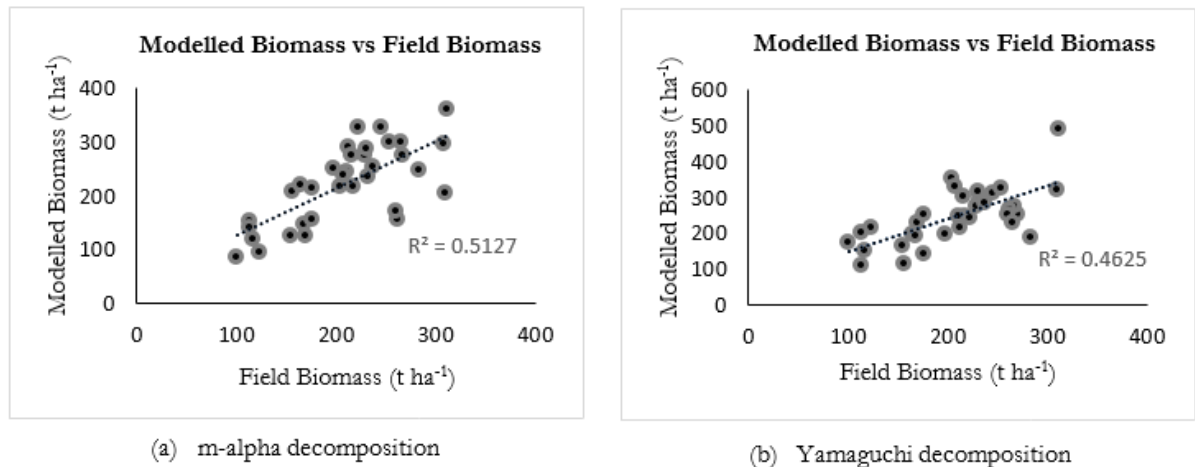


Figure 5-21: (a) Modelled AGB using m-alpha decomposition against field biomass (b) Modelled AGB using Yamaguchi decomposition against field biomass

The Figure 5-20 (a), Figure 5-20 (b), Figure 5-21 (a) and Figure 5-21 (b) are showing correlation between modelled AGB and field biomass. All the scatterplots are showing positive correlation between modelled AGB and field biomass. Using polarimetric decomposition components of m-delta decomposition for modelling AGB is showing R^2 value as 0.3977 with field biomass. The R^2 value for modelling AGB using

m-chi decomposed components with field biomass is 0.4677. The R² value using m-alpha decomposed components for modelling AGB with field biomass is 0.5127. Using Yamaguchi decomposed components for modelling AGB is showing R² value as 0.4625 with field measured biomass.

5.7. Performance Analysis

The performance of parameters derived from modelling approach is verified using field measured data. The accuracy of the modelled AGB is estimated using field measured biomass.

The Root Mean Square Error (RMSE) is calculated for the modelled AGB with respect to biomass measured in the field with the help of given formula.

$$RMSE = \sqrt{\frac{\sum_{i=1}^N (AGB_{modelled(i)} - AGB_{measured(i)})^2}{N}} \quad (5.4)$$

Where, N represents number of sample plots, $AGB_{modelled}$ represents modelled AGB and $AGB_{measured}$ represents the field measured biomass. Here the value of N is 39.

Table 5-2. RMSE obtained for modelled AGB and field biomass

Modelled AGB	<i>RMSE</i> (t ha ⁻¹)			
	m-delta	m-chi	m-alpha	Yamaguchi
	Decomposition	Decomposition	Decomposition	Decomposition
	64.422	45.995	63.156	73.424

The Table (5-2) represents that using EWCM the modelled AGB for m-delta, m-chi, m-alpha and Yamaguchi decomposition is 64.422 (t ha⁻¹), 45.995 (t ha⁻¹), 63.156 (t ha⁻¹) and 73.424 (t ha⁻¹) respectively. The RMSE of m-delta and m-alpha is nearly equal. The RMSE of Yamaguchi is higher than other i.e. 73.424 (t ha⁻¹) while the RMSE of m-chi decomposition is lower i.e. 45.995 (t ha⁻¹).

The accuracy of modelled AGB is calculated for all the decomposition like m-delta, m-alpha, m-chi and Yamaguchi. The accuracy represents how much closer the modelled AGB follows field measured biomass. The formula for percent accuracy can be given as

$$Accuracy (\%) = \left[1 - \frac{\sqrt{\frac{1}{N} \sum_{i=1}^N (AGB_{modelled(i)} - AGB_{measured(i)})^2}}{AGB_{measured(i)}} \right] \times 100 \quad (5.5)$$

Where, $AGB_{measured}$ = Biomass measured in the field

$AGB_{modelled}$ = Estimated AGB using modelling approach

The Table (5-3) represents the percent accuracy obtained in the modelled AGB using m-delta, m-chi, m-alpha and Yamaguchi decomposed components.

Table 5-3. Percent accuracy for modelled AGB

Modelled AGB	<i>Accuracy (%)</i>			
	m-delta	m-chi	m-alpha	Yamaguchi
	Decomposition	Decomposition	Decomposition	Decomposition
	71.01	79.30	71.58	66.96

The m-delta decomposition is showing 71.01% accuracy in modelled biomass with respect to field measured biomass. The m-chi decomposition is showing 79.30% accuracy. Modelled biomass is showing 71.58% accuracy with field measured biomass in m-alpha decomposition while Yamaguchi decomposition is showing 66.96% accuracy in aspect of modelled biomass and field measured biomass. The modelled biomass using m-chi decomposed components is showing better accuracy as 79.30% while modelled AGB using Yamaguchi decomposed components is showing less accuracy 66.96% than remaining decomposition methods.

6. DISCUSSION

The present chapter deals with the discussion related to the results obtained and the analysis done to find out the best possible reasons concerning the results.

This research work deals with the estimation of AGB using hybrid polarimetric data and fully polarimetric data. The interpretation of the outcomes attained using hybrid PolSAR data i.e. RISAT-1 and fully polarimetric data i.e. Radarsat-2 forms the basis of this study. This hybrid polarimetric data is used for decomposition modelling and for the estimation of above ground biomass. Various inferences are drawn based on the analysis of the results. The discussion of the results is done in four parts corresponding to the four objectives.

Hybrid PolSAR data and fully polarimetric SAR data were used to obtain the scattering elements i.e. surface scattering, volume scattering and double-bounce scattering. Three types of decomposition techniques were used for the hybrid polarimetric data namely, m-delta, m-chi and m-alpha. For each of the decomposition technique scattering elements were obtained. For the given study area volume scattering dominates the surface scattering and double-bounce scattering for m-delta decomposition technique as shown in figure 5-3. This is due to the fact that the present study area is conquered by the dense forest. Hence, most of the scattering occurs in the upper canopy layer. The similar pattern is observed for all three types of decomposition techniques i.e. m-delta, m-chi and m-alpha and for fully polarimetric data as well.

Previous research work dealt with extraction of scattering elements using m- delta and m-chi decomposition techniques. Raney *et al.*, in [71] showed that m-delta decomposition produced anomalous results in retrieval of scattering elements for lunar surface. Saran *et al.*, [72] used m-chi decomposition for retrieval of scattering elements from lunar surface and found significant results. The decomposition based modelled output were compared for each of the scattering element i.e. surface scattering, double-bounce scattering and volume scattering. For volume scattering maximum backscatter value was found to be 0.899, 0.833, 0.732 and 0.846 for m-delta, m-chi, m-alpha and Yamaguchi decomposition respectively. On the other hand the backscatter values were found to be very low for rest of the two scattering elements i.e. surface scattering and double-bounce scattering. The backscatter value of volume scattering for all decompositions are nearly close to each other. The reason may be that degree of polarization (m) is sensitive indicator of volume scattering which is same for all the hybrid polarimetric decompositions i.e. m-delta, m-chi and m-alpha. As the Barkot forest area is densely packed with the canopy cover hence, the incoming C-band waves first interact with the top canopy layer giving high values for the volume scattering. On the other hand, some of the waves may penetrate through the canopy layer and double bounce scattering occur due to ground stem interactions or stem ground interactions. Also, due to the canopy gaps surface scattering may also occur. But the present study area is composed of quite dense forest hence volume scattering is dominating.

A semi-empirical model i.e. EWCM was used to estimate AGB for both types of datasets i.e. hybrid polarimetric data and fully polarimetric data. The parameters required for AGB calculation was determined using polarimetric decomposition techniques such as m-delta, m-chi, m-alpha and Yamaguchi decomposition.

The scatter plots are used for the analysis of the results. Figure 5-16 and Figure 5-17 compares the volume scattering with the field biomass data collected during the field work in the Barkot forest area. For polarimetric decomposition such as m-delta, m-chi, m-alpha, backscatter values of volume scattering shows weak correlation with field measured biomass. The reason may be that there is not much increment in the field measured biomass as the field measured biomass for most of the plots generally ranges between 200 ($t\ ha^{-1}$) to 250 ($t\ ha^{-1}$). Hence for those plots the volume scattering is generally similar to field measured biomass ranging from 200 ($t\ ha^{-1}$) to 250 ($t\ ha^{-1}$). Whereas, the backscatter values of volume scattering increases with the field measured biomass for fully polarimetric data. The reason may be that before deorientation of fully polarimetric data, the volume scattering is overestimated. In Figure 5-18 and Figure 5-19, the correlation between total forest backscatter and the field measured biomass has been depicted. For all the three decompositions i.e. m-delta, m-chi and m-alpha there is not much variation in total backscatter with respect to the field measured biomass. The reason may be that the C-band wavelength used for the present study penetrates the forest area to a lesser extent which affects the total forest backscatter. On the contrary, total backscatter increases with the increase in the field biomass for fully polarimetric data and showing positive correlation. The reason for this is that with the increase in AGB the volume scattering also increases which leads to elevated values of total backscatter. Hence, the AGB shows linear relationship with the total forest backscatter values.

The AGB calculated with the help of semi-empirical model was compared with the field data. On comparison it was found that the m-alpha decomposition shows highest correlation i.e. 0.5129 among others i.e. m-delta, m-chi and Yamaguchi decompositions. The purpose of comparison between the modelled biomass and the field biomass is carried out to find the relation between the modelled values and the actual ground values. Although the volume scattering, the total backscatter and the biomass shows weak correlation but there is a positive correlation between modelled biomass and the field biomass which comes out to be quite high. This is due to the plots used in present study are quite homogeneous giving high field biomass. Due to the dense forest the volume scattering comes out to be high leading to high total backscatter. This gives high values of modelled AGB calculated using semi-empirical model i.e. EWCM. Hence there exists a positive and linear correlation between modelled AGB and field biomass.

The study conducted by Chandola [17] depicted that the R^2 values between volume scattering using Yamaguchi decomposition against field biomass (for the 45 plots) for master image as 0.457 and for slave image as 0.471. Whereas, R^2 values in the present study for volume scattering using Yamaguchi

decomposition against field biomass is 0.4244. The R^2 value in research work by Chandola [17] for total backscatter against field biomass for master and slave image was 0.468 and 0.24 respectively but for the current study R^2 value came out to be 0.28. The comparison between modelled biomass against field biomass showed R^2 value as 0.496 [17] using IWCM and 0.4625 (for present study) using EWCM. The reason for this disparity may be due to the seasonal variations in the data and difference in the number of plots taken for the same study area Barkot forest. The variations in results are also due to the different models used for AGB estimation.

At last performance analysis is done by calculating RMSE for modelled AGB with respect to the biomass measured in the field. The decomposition model that performed best was m-chi decomposition technique with RMSE of 45.995 ($t\ ha^{-1}$). The m-chi decomposition technique also performed significantly for lunar surface in differentiating the even-bounce backscatter against odd-bounce backscatter as concluded in research work by Bhavya [73]. Yamaguchi decomposition performed worst giving the RMSE of 73.424 ($t\ ha^{-1}$). The best accuracy was 79.30% for m-chi decomposition. Least accuracy was corresponding to the Yamaguchi decomposition i.e. 66.96%. The other two decomposition models i.e. m-delta and m-alpha performed at par with 71.01% and 71.58% accuracy. These performance analysis results are summarized in Table (5-2) and (5-3). The variation in the results obtained from each decomposition may be due to the parameters (m , δ , χ and α) considered for decomposition modelling.

7. CONCLUSION AND RECOMMENDATIONS

7.1. Conclusion

The prime objective of this research was to evaluate the potential of Hybrid PolSAR for implying decomposition modelling to estimate the AGB as stated in first chapter.

A model based approach was used to estimate AGB. Water Cloud Model was used to retrieve the forest stand parameter i.e. AGB and which is a semi-empirical model. This model was extended for the ground to stem interactions and applied in this study as Extended Water Cloud Model. This model was trained using 49 plots. Out of 49 plots, 15 plots were taken to estimate the semi-empirically defined coefficient with the help of *in-situ* measurements. Remaining 34 plots were used to estimate the AGB. Precise estimates of backscatter from vegetation, backscatter from ground to stem interactions, backscatter from ground surface were obtained. The model well described the relation of backscatter values with the field measured biomass.

Total four decomposition models were used to retrieve the scattering elements. Three decomposition modelling approach were used for Hybrid PolSAR data and one for fully PolSAR data. Hybrid PolSAR decomposition modelling used in this study are m-delta decomposition, m-chi-decomposition and m-alpha decomposition. Decomposition method for fully PolSAR data which was used in this study was Yamaguchi four component decomposition modelling.

AGB estimation using Extended Water Cloud Model for m-delta decomposition showed R^2 value as 0.3977. The estimate RMSE was found as 64.422 ($t\ ha^{-1}$). On the basis of the results obtained from this decomposition method, the accuracy was found to be 71.01%. The m-chi decomposition showed R^2 value as 0.4677 for modelled biomass. The RMSE was calculated and found to be 45.995 ($t\ ha^{-1}$). The calculated accuracy for m-chi decomposition was 79.30%. The m-alpha decomposition showed R^2 value as 0.5127 for AGB estimation with estimated RMSE was 63.156 ($t\ ha^{-1}$). The accuracy for m-alpha decomposition was found as 71.58%.

Another statistical measure was used for the analysis of the results i.e. correlation coefficient (R). It shows the relationship between two quantities. On comparison of the correlation coefficient values, it was found that the R values were nearly close for m-chi, Yamaguchi and m-alpha decomposition. Although the m-chi and m-alpha varied significantly. There was a huge difference in the values of RMSE for m-chi, Yamaguchi and m-alpha decomposition as 45.995 ($t\ ha^{-1}$), 73.424 ($t\ ha^{-1}$) and 63.156 ($t\ ha^{-1}$) respectively. Since the RMSE value for m-chi is lowest among all, hence m-chi outperformed all other decompositions.

7.2. Answers to Research Questions

- a) What will be the significance of Stokes parameters for scattering element retrieval using Hybrid PolSAR data?

Scattering element retrieval using Hybrid PolSAR data depends on the parameters used in the Hybrid PolSAR decomposition technique (\mathbf{m} , δ , χ and α) and Stokes first parameter (S_1). The volume scattering is sensitively indicated by \mathbf{m} , Characterization of even bounce against odd bounce is sensitively indicated by δ (in \mathbf{m} - δ decomposition) and χ (in \mathbf{m} - χ decomposition) and α shows the scattering mechanism. All these parameters ultimately depend on Stokes parameter. Hence, variation in the Stokes parameter value affects the contribution of scattering element in the Hybrid PolSAR decomposition technique.

- b) Which decomposition techniques can be used for retrieval of surface, double bounce and volume scattering information using Hybrid pol data?

There are three decomposition techniques that can be used for retrieval of surface, double bounce and volume scattering information using Hybrid pol data which was based on four parameters i.e. \mathbf{m} , δ , χ and α . They are \mathbf{m} - δ , \mathbf{m} - χ and \mathbf{m} - α decomposition.

- c) How to retrieve semi-empirical modelling parameters from Hybrid PolSAR data for AGB estimation?

There are four unknown parameters in semi-empirical modelling like EWCM (used in this study). They are backscatter from ground surface, backscatter from ground to stem interactions or stem to ground interactions, backscatter from vegetation and semi-empirically defined coefficient which are then reduced to one i.e. semi-empirically defined coefficient. The remaining semi-empirical modelling parameters retrieved by using decomposition techniques for Hybrid PolSAR data. The field measured biomass of 15 plots and decomposition components obtained from Hybrid PolSAR data are then used to estimate the semi-empirically defined coefficient.

- d) To what extent the scattering information retrieved from Hybrid PolSAR differ from fully polarimetric SAR?

The backscatter values of volume scattering for hybrid PolSAR data was more than the backscatter values of volume scattering obtained using fully polarimetric data before deorientation. The backscatter values of volume scattering were found to be 0.899, 0.833 and 0.732 for \mathbf{m} - δ , \mathbf{m} - χ and \mathbf{m} - α . For Yamaguchi decomposition the backscatter values of same scattering was found to be 0.846.

- e) How viable is the Hybrid PolSAR techniques for the estimation of AGB in comparison to the results obtained from fully PolSAR based AGB estimation and field data?

On comparing the accuracy assessment results it was found that hybrid polarimetric data is more viable for AGB estimation than before deoriented fully polarimetric data. This is based on the fact that RMSE was 64.422 (t ha⁻¹), 45.995 (t ha⁻¹) and 63.156 (t ha⁻¹) for m-delta, m-chi and m-alpha respectively. For Yamaguchi decomposition the RMSE was 73.424 (t ha⁻¹). The correlation coefficient values were 0.63063, 0.6838, 0.7160 and 0.68007 for m-delta, m-chi, m-alpha and Yamaguchi decomposition respectively. The percentage accuracy for modelled ABG was 71.01%, 79.30% and 71.58% for m-delta, m-chi and m-alpha respectively. Whereas, Yamaguchi decomposition gave an accuracy of 66.96%. On the basis of statistical parameter i.e. correlation coefficient, RMSE and percent accuracy, the m-chi decomposition was found to be better than other decompositions for the estimation of AGB.

7.3. Recommendations

To further improve this research work for increasing the consistency of decomposition modelling for AGB estimation, some of the recommendations are enlisted below.

- The current research work used Hybrid PolSAR data with C-band for estimating AGB. The L-band data can also be used for enhancing the AGB estimation as the longer wavelength would affect the results.
- The present work was carried out in Barkot forest which is a homogeneous forest assisted by Sal and mix Sal to estimate the potential of Hybrid polarimetric decomposition modelling. The decomposition modelling can also be tested for heterogeneous forest to check the reliability of modelling approach.
- The current research focuses on the generation of Stokes parameters for retrieving the scattering information for the Hybrid polarimetric decomposition modelling. A pseudo quad pol method should also be implied for retrieving scattering information using decomposition modelling.
- In this research work semi-empirical modelling was applied to estimate the AGB. A regression approach should also be tried to estimate and analyses the AGB.

REFERENCES

- [1] “The Forest Biome,” 2014. Available: <http://www.ucmp.berkeley.edu/exhibits/biomes/forests.php>. [Accessed: 12-Jan-2015]
- [2] S. Brown, “*Estimating Biomass and Biomass Change of Tropical Forests: A Primer.*” Food & Agriculture Org., 1997, p. 72.
- [3] S. Kumar, “Retrieval of forest parameters from Envisat ASAR data for biomass inventory in Dudhwa National Park, U.P., India,” International Institute for Geo-information Science and Earth Observaton (ITC), 2009.
- [4] Securing Forests Securing Rights, “Report of the International Workshop on Deforestation and the Rights of Forest.” Forest People Programme, March. 2014, pp. 1–132. Available: <http://www.forestpeoples.org/topics/rights-land-natural-resources/publication/2014/securing-forests-securing-rights-report-intern>. [Accessed 25-Jan-2015]
- [5] S. Chao, “Forest Peoples: numbers across the world.” Forest People Programme, United Kingdom 2012.
- [6] M. Santoro, C. Beer, O. Cartus, C. Schmullius, A. Shvidenko, I. McCallum, U. Wegmüller, and A. Wiesmann, “Retrieval of growing stock volume in boreal forest using hyper-temporal series of Envisat ASAR ScanSAR backscatter measurements,” *Remote Sens. Environ.*, vol. 115, no. 2, pp. 490–507, Feb. 2011.
- [7] I. H. Woodhouse, “*Introduction to Microwave Remote Sensing.*” CRC Press, Boca Raton, 2005, p. 410.
- [8] H. G. Jones and R. A. Vaughan, *Remote Sensing of Vegetation*, ”First. Oxford University Press Inc., New York, 2010, pp. 107–115.
- [9] M. E. Nord, T. L. Ainsworth, S. Member, J. Lee, L. Fellow, and N. J. S. Stacy, “Comparison of Compact Polarimetric Synthetic Aperture Radar Modes,” *IEEE Trans. Geosci. Remote Sens.*, vol. 47, no. 1, pp. 174–188, 2009.
- [10] A. Freeman and S. L. Durden, “A Three-Component Scattering Model for Polarimetric SAR Data,” *IEEE Trans. Geosci. Remote Sens.*, vol. 36, no. 3, pp. 963–973, 1998.
- [11] J. P. M. Overman, H. J. L. Witte, and J. G. Saldarriaga, “Evaluation of Regression Models for Above-Ground Biomass Determination in Amazon Rainforest,” *J. Trop. Ecol.*, vol. 10, no. 2, pp. 207–218, 1994.
- [12] R. K. Raney, “Hybrid-Polarity SAR Architecture,” *IEEE Trans. Geosci. Remote Sens.*, vol. 45, no. 11, pp. 3397–3404, 2007.
- [13] T. L. Ainsworth, J. P. Kelly, and J.-S. Lee, “Classification comparisons between dual-pol, compact polarimetric and quad-pol SAR imagery,” *ISPRS J. Photogramm. Remote Sens.*, vol. 64, no. 5, pp. 464–471, Sep. 2009.
- [14] R. K. Raney, “Decomposition of Hybrid-Polarity SAR Data,” in *PolInSAR 2007: Proceedings of the 3rd International Workshop on Science and Applications*, 2007, pp. 22–26.

- [15] J. Lee and T. L. Ainsworth, "The Effect of Orientation Angle Compensation on Coherency Matrix and Polarimetric Target Decompositions," *IEEE Trans. Geosci. Remote Sens.*, vol. 49, no. 1, pp. 53–64, 2011.
- [16] U. Khati, S. Kumar, and D. P. Thakur, "Effect of Shift in Polarization Orientation Angle on Multi-wavelength Fully Polarimetric Data," in *9th International Conference on Microwaves, Antenna, Propagation and Remote Sensing (ICMARS)*, 2013, vol. 1, no. 1, pp. 30–34.
- [17] S. Chandola, "Polarimetric SAR Interferometry for Forest Aboveground Biomass Estimation," Faculty of Geoinformation and Earth Science, University of Twente, 2014.
- [18] S. Englhart, V. Keuck, and F. Siegert, "Aboveground biomass retrieval in tropical forests — The potential of combined X- and L-band SAR data use," *Remote Sens. Environ.*, vol. 115, no. 5, pp. 1260–1271, May 2011.
- [19] N. Ghasemi, M. R. Sahebi, and A. Mohammadzadeh, "A review on biomass estimation methods using synthetic aperture radar data," *Int. J. Geomatics Geosci.*, vol. 1, no. 4, pp. 776–788, 2011.
- [20] S. Kumar, U. Pandey, S. P. Kushwaha, R. S. Chatterjee, and W. Bijker, "Aboveground biomass estimation of tropical forest from Envisat advanced synthetic aperture radar data using modeling approach," *J. Appl. Remote Sens.*, vol. 6, no. 1, p. 063588, Oct. 2012.
- [21] S. Kumar, U. Pandey, S. P. S. Kushwaha, and R. S. Chatterjee, "Aboveground biomass estimation of tropical forest from Envisat ASAR data using modeling approach," *J. Appl. Remote Sens.*, vol. 6, pp. 1–18, 2012.
- [22] SAI. B. Poolla, "Polarimetric scattering model for biophysical characterization of multilayer vegetation using space borne PolSAR data," Faculty of Geoinformation Science and Earth Observation, University of Twente, 2013.
- [23] A. Kangas and M. Maltamo, "*Forest Inventory: methodology and applications*," vol. 10. Springer Science & Business Media, 2006, p. 364.
- [24] B. Husch, T. W. Beers, and J. A. Kershaw, "*Forest Mensuration*," Fourth. John Wiley & Sons, Inc., Hoboken, New Jersey, 2003, pp. 314–316.
- [25] B. Husch, C. I. Millar, and T. W. Beers, "*Forest Mensuration*," Second. The Ronald Press Company, New York, 1971, pp. 224–226.
- [26] M. A. Wulder, J. C. White, R. A. Fournier, J. E. Luther, and S. Magnussen, "Spatially Explicit Large Area Biomass Estimation: Three Approaches Using Forest Inventory and Remotely Sensed Imagery in a GIS," vol. 8, pp. 529–560, 2008.
- [27] M. A. Lefsky, W. B. Cohen, G. G. Parker, and D. J. Harding, "Lidar Remote Sensing for Ecosystem Studies," *Bioscience*, vol. 52, no. 1, pp. 19–30, 2002.
- [28] D. Lu, Q. Chen, G. Wang, E. Moran, M. Batistella, M. Zhang, G. V. Laurin, and D. Saah, "Aboveground Forest Biomass Estimation with Landsat and LiDAR Data and Uncertainty Analysis of the Estimates," *Int. J. For. Res.*, vol. 2012, no. 1, p. 16, 2012.
- [29] A. Jochem, M. Hollaus, M. Rutzinger, and B. Höfle, "Estimation of aboveground biomass in alpine forests: a semi-empirical approach considering canopy transparency derived from airborne LiDAR data," *Sensors (Basel)*, vol. 11, no. 1, pp. 278–95, Jan. 2011.

- [30] M. A. Tanase, R. Panciera, K. Lowell, C. Aponte, J. M. Hacker, and J. P. Walker, "Forest Biomass Estimation at High Spatial Resolution : Radar Versus Lidar Sensors," *IEEE Geosci. Remote Sens. Lett.*, vol. 11, no. 3, pp. 711–715, 2014.
- [31] S. Hensley, S. Oveisgharan, S. Saatchi, M. Simard, R. Ahmed, and Z. Haddad, "An Error Model for Biomass Estimates Derived From Polarimetric Radar Backscatter," *IEEE Trans. Geosci. Remote Sens.*, vol. 52, no. 7, pp. 4065–4082, 2014.
- [32] G. Sandberg, L. M. H. Ulander, J. Wallerman, and J. E. S. Fransson, "Measurements of Forest Biomass Change Using P-Band Synthetic Aperture Radar Backscatter," *IEEE Trans. Geosci. Remote Sens.*, vol. 52, no. 10, pp. 6047–6061, 2014.
- [33] K. O. Pope, J. M. Rey-Benayas, and J. F. Paris, "Radar remote sensing of forest and wetland ecosystems in the Central American tropics," *Remote Sens. Environ.*, vol. 48, no. 2, pp. 205–219, May 1994.
- [34] M. a. Tanase, R. Panciera, K. Lowell, S. Tian, J. M. Hacker, and J. P. Walker, "Airborne multi-temporal L-band polarimetric SAR data for biomass estimation in semi-arid forests," *Remote Sens. Environ.*, vol. 145, pp. 93–104, Apr. 2014.
- [35] R. K. Panigrahi and A. K. Mishra, "Comparison of hybrid-Pol with quad-Pol scheme based on polarimetric information content," *Int. J. Remote Sens.*, vol. 33, no. 11, pp. 3531–3541, Jun. 2012.
- [36] J. Souyris, P. Imbo, R. Fjørtoft, S. Mingot, and J. Lee, "Compact Polarimetry Based on Symmetry Properties of Geophysical Media : The $\pi/4$ Mode," *IEEE Trans. Geosci. Remote Sens.*, vol. 43, no. 3, pp. 634–646, 2005.
- [37] L. Ferro-famil and E. Pottier, "Radar Polarimetry Basics and Selected Earth Remote Sensing Applications," in *Academic Press Library in Signal Processing: Volume 2-Communications and Radar Signal Processing*, vol. 2, Elsevier, 2014, pp. 1119–1244.
- [38] B. Souissi, M. Ouarzeddine, and A. Belhadj-aissa, "Investigation of the capability of the Compact Polarimetry mode to Reconstruct Full Polarimetry mode using RADARSAT2 data," *Adv. Electromagn.*, vol. 1, no. 1, pp. 21–28, 2012.
- [39] "Polarimetric Decompositions." Available: https://earth.esa.int/documents/653194/656796/Polarimetric_Decompositions.pdf. Accessed[5-Jan-2015]
- [40] E. Krogager, "New Decomposition of the Radar Target Scattering Matrix," *Electron. Lett.*, vol. 26, no. 18, pp. 1525–1527, 1990.
- [41] S. R. Cloude and E. Pottier, "A Review of Target Decomposition Theorms in Radar Polarimetry," *IEEE Trans. Geosci. Remote Sens.*, vol. 32, no. 2, pp. 498–518, Jun. 1996.
- [42] Y. Oh and J. H. S. Lee, "A Simple Microwave Backscattering Model for Vegetation Canopies," *Journal Korea Electromagn. Eng. Soc.*, vol. 5, no. 4, pp. 183–188, 2005.
- [43] J. D. B. Berman and J. M. L. Sanchez, "Application of Freeman-Durden Decomposition to Polarimetric SAR Interferometry Decomposition of the correlation matrix C_{int} ," *EUSAR*, pp. 805–808, 2010.

- [44] D. Gaglione, C. Clemente, L. Pallotta, I. Proudler, A. De Maio, J. J. Soraghan, and G. Street, “Krogager Decomposition and Pseudo-Zernike Moments for Polarimetric Distributed ATR,” *IEEE*, pp. 1–5, 2014.
- [45] P. V. Jayasri, H. S. V. U. Sundari, E. V. S. Sita, and A. V. V. Prasad, “M-delta Decomposition of Hybrid Dual- Polarimetric RISAT-1 SAR Data,” *9th Int. Radar Symp.*, vol. IRSI-13, no. December, pp. 1–4, 2013.
- [46] V. Turkar, S. De, G. G. Ponnurangam, R. Deo, Y. S. Rao, and A. Das, “Classification of RISAT-1 Hybrid Polarimetric Data for Various Land Features,” pp. 1–4, 2012.
- [47] E. P. W. Attema and F. T. Ulaby, “Vegetation modeled as a water cloud,” *Radio Sci.*, vol. 13, no. 2, pp. 357–364, 1978.
- [48] L. Liu, Y. Shao, K. Li, H. Gong, and A. T. V. Model, “A Two Layer Water Cloud Model,” *IEEE Geosci. Remote Sens. Lett.*, no. 3, pp. 5840–5843, 2012.
- [49] M. Bracaglia, P. Ferrazzoli, and L. Guerriero, “A Fully Polarimetric Multiple Scattering Model for Crops,” *Remote Sens. Environ.*, vol. 54, pp. 170–179, 1995.
- [50] X. Zhou and M. A. Hemstrom, “Estimating Aboveground Tree Biomass on Forest Land in the Pacific Northwest : A Comparison of Approaches,” no. November, 2009.
- [51] J. C. Jenkins, D. C. Chojnacky, L. S. Heath, and R. A. Birdsey, “National-Scale Biomass Estimators for United States Tree Species,” *For. Sci.*, vol. 49, pp. 12–35, 2003.
- [52] K. Kumar, K. S. Hari Prasad, and M. K. Arora, “Estimation of water cloud model vegetation parameters using a genetic algorithm,” *Hydrol. Sci. J.*, vol. 57, no. 4, pp. 776–789, May 2012.
- [53] S. Enghart, S. Member, V. Keuck, and F. Siegert, “Modeling Aboveground Biomass in Tropical Forests Using Multi-Frequency SAR Data — A Comparison of Methods,” *IEEE J. Sel. Top. Appl. Earth Obs. Remote Sens.*, vol. 5, no. 1, pp. 298–306, 2012.
- [54] I. E. E. Report, “Infrastructure Development Investment Program for Tourism - Tranche 2,” India, 2014.
- [55] Forest Survey of India, “*Volume Equations for Forests of India, Nepal and Bhutan.*,” vol. 501, no. c. Ministry of Environment and Forests, Dehradun, India, 1996, pp. 1–249.
- [56] V. D. Limaye and B. R. Sen, “*Weight and Specific Gravity of Indian Woods.*” Forest Reseach Institute, Indian Forest Records, vol. I-VI, Dehradun, India, 1956.
- [57] W. Boerner, “Basics of Radar Polarimetry I,” Pol SARpro V3.0 – Lecture Notes.
- [58] W.-M. Boerner, *Principles of Optics*, 3rd Editio. Pergamon Press, NewYork, 1965, p. 808.
- [59] R. K. Raney, “M-chi Decomposition of Imperfect Hybrid Dual-Polarimetric Radar Data,” *6th Int. Work. Sci. Appl. SAR Polarim. Polarim. Interferom. Eur. Sp. Agency, Frascati, Italy*, 2013.
- [60] S. Cloude, “*Polarization: Applications in Remote Sensing.*” Oxford University Press, USA, 2009.

- [61] L. J. V. Kumar, J. K. Kishore, and P. K. Rao, "Decomposition Methods for Detection of Oil Spills Based on RISAT-1 SAR Images Decomposition Methods for Detection of Oil," *Int. J. Remote Sens. Geosci.*, vol. 3, no. 4, 2014.
- [62] W. M. Boerner, "Basic Concepts in Radar Polarimetry," Chicago, USA, 1998.
- [63] R. Touzi, W. M. Boerner, J. S. Lee, and E. Lueneburg, "A Review of Polarimetry in the Context of Synthetic Aperture Radar: concepts and information extraction," *Can. J. Remote Sens.*, vol. 30, no. 3, pp. 380–407, 2004.
- [64] J. S. Lee and E. Pottier, *Polarimetric radar imaging: from basics to applications*. Boca Raton: CRC Press, 2009, pp. 1–10.
- [65] Y. Yamaguchi, Y. Yajima, and H. Yamada, "A Four-Component Decomposition of POLSAR Images Based on the Coherency Matrix," *IEEE Geosci. Remote Sens. Lett.*, vol. 3, no. 3, pp. 292–296, Jul. 2006.
- [66] Y. Yamaguchi, T. Moriyama, M. Ishido, and H. Yamada, "Four Component Scattering Model for Polarimetric SAR image decomposition," *IEEE Trans. Geosci. Remote Sens.*, vol. 43, no. 8, pp. 1699–1706, 2005.
- [67] M. Santoro, J. Askene, G. Smith, and J. E. Fransson, "Stem Volume retrieval in boreal forests from ERS-1/2 interferometry," *Remote Sens. Environ.*, vol. 81, no. 1, pp. 19–35, 2002.
- [68] M. Santoro, L. Eriksson, J. Askne, and C. Schmullius, "Assessment of stand-wise stem volume retrieval in boreal forest from JERS-1 L-band SAR backscatter," *Int. J. Remote Sens.*, vol. 27, no. 16, pp. 3425–3454, Aug. 2006.
- [69] M. Santoro, L. Eriksson, J. Askne, and C. Schmullius, "Assessment of Stand-Wise Stem Volume Retrieval in Boreal Forest from JERS-1 L-band SAR backscatter," *Int. J. Remote Sens.*, vol. 27, no. 16, pp. 3425–3454, 2006.
- [70] J. A. Richards, G.-Q. Sun, and D. S. Simonett, "L-Band Forest Stands," *IEEE Trans. Geosci. Remote Sens.*, vol. GE-25, no. 4, pp. 487–498, 1987.
- [71] R. K. Raney, J. T. S. Cahill, G. W. Patterson, and D. B. J. Bussey, "The m-chi decomposition of hybrid dual-polarimetric radar data," *J. Geophys. Res.*, vol. 117, no. E5, pp. 5093–5096, 2012.
- [72] S. Saran, A. Das, S. Mohan, and M. Chakraborty, "Study of Scattering Characteristics of Lunar Equatorial Region using Chandrayaan-I Mini-SAR Polarimetric Data," *Planet. Space Sci.*, vol. 71, no. 1, pp. 18–30, 2012.
- [73] K. B. Bhavya, "Polarimetric Modeling of Lunar Surface for Scattering Information Retrieval Using Mini-SAR Data of Chandrayaan-1," Faculty of Geo-information Science and Earth Observation, University of Twente, 2013.

APPENDIX A

The Poincaré Polarization Sphere:

Any quasi monochromatic wave may be represented using Stokes parameter (S_1 , S_2 , S_3 and S_4). The polarization of a wave using these parameters can be represented by Poincaré sphere (Figure A-1). This representation helps in visualizing the polarization effects. These Stokes parameter can be observed as the cartesian coordinates of a point on a sphere (Poincaré sphere) which determines a specific location on the conceptual spherical surface analogous to the polarized portion of the wave. Hence, represents a unique mapping location of a point on sphere and a polarization state.

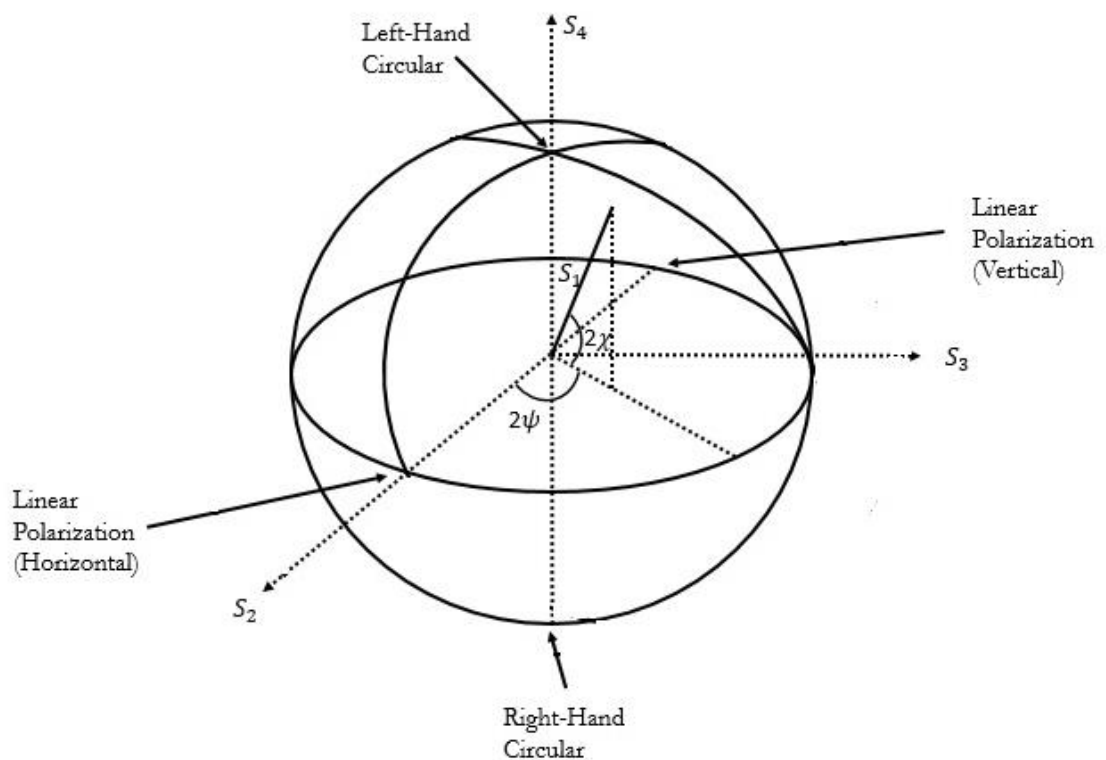


Figure A-1: The Poincaré Sphere

The Figure A-1 represents the mapping between location of a point on the surface of sphere and polarization state as;

- Linear polarization map to points on the equator.
- Circular polarization map to points on the poles.
- Orthogonal polarization are anti-podal means map to points on opposite side of the sphere.